Title: Mind the blank: behavioral, experiential, and physiological signatures of absent-mindedness

Authors: Esteban Munoz Musat[1], Andrew W. Corcoran[2], Laouen Belloli[1], Lionel Naccache[1,3], Thomas Andrillon[1,2,4*]

Affiliations:

[1] Paris Brain Institute, Sorbonne Université, Inserm-CNRS, Paris, France
[2] Monash Centre for Consciousness and Contemplative Studies, Faculty of Arts, Monash University, Melbourne, Australia
[3] Service de Neurophysiologie, Hôpital Pitié Salpêtrière, Paris, France
[4] Service des Pathologies du Sommeil, Hôpital Pitié Salpêtrière, Paris, France
*Corresponding author. Email: thomas.andrillon@icm-institute.org.

ABSTRACT:

Does being awake mean being conscious? This study investigates Mind Blanking (MB), characterized by an "emptiness of mind", comparing it with Mind Wandering (MW) and On-task (ON) states. Using a sustained attention task and electroencephalogram monitoring on 26 participants, behavioral and neurophysiological signatures of MB were examined. MB exhibited a specific pattern of behavioral lapses, as well as decreased fast oscillatory activity and complexity over posterior electrodes compared to MW. Functional connectivity analyses also revealed decreased frontal-posterior connectivity during MB and event-related potentials indicated a disruption in late-stage visual processing, suggesting a lack of conscious access to sensory information during MB. EEG-based neural features enabled trial-level prediction of mental states, furnishing estimates of the fine-grained dynamics of consciousness beyond subjective reports. Overall, these findings challenge the notion of continuous wake consciousness, suggesting that MB represents genuine gaps in our stream of thoughts.

SIGNIFICANCE STATEMENT:

Employing cutting-edge neurophysiological techniques on high-density EEG recordings, our study unveils unique neurophysiological markers of mind blanking—a phenomenon characterized by lapses in conscious content amidst the flow of consciousness. Distinguished from task-oriented states and mind wandering, this signature sheds light on the elusive nature

of mind blanking. Furthermore, we demonstrate the feasibility of decoding consciousness dynamics solely from EEG features, transcending the limitations of intermittent subjective reports. Our findings not only provide a novel framework for investigating the stream of consciousness but also challenge the conventional notion that wakefulness invariably signifies consciousness.

Keywords: Mind Blanking, Mind Wandering, EEG, Neurophysiology, Consciousness, Attention.

INTRODUCTION

> *"Consciousness, then, does not appear to itself chopped up in bits. Such words as 'chain' or 'train' do not describe it fitly as it presents itself in the first instance. It is nothing jointed; it flows. A 'river' or a 'stream' are the metaphors by which it is most naturally described. In talking of it hereafter let us call it the stream of thought, of consciousness, or of subjective life"* (William James, 1890).

In the former quote, William James pointed to two very intuitive aspects of our conscious experience[1]. First, consciousness seems indeed *continuous* during wakefulness, without any "pauses" or breaks. Second, our conscious experience is dynamic and conscious content changes very frequently.

Regarding this last point, previous research has shown indeed that our conscious cognitive resources can be directed toward the external world and enable the selection and amplification of information relevant to our current behavioral goals[2]. But our consciousness can also turn inward, as is the case when we focus on internally generated task-unrelated thoughts, a phenomenon usually referred to as mind wandering (MW)[3,4]. Extensive research has shown that, in the brain, the transitions between task-related focus and MW involve modulations of activity of the Default-mode network (DMN)[5] as well as changes in cortical dynamics with modulations of alpha activity[6,7] and increases in slower rhythms[8].

More recently, a third "mind state" has been described, challenging the idea of a continuous conscious experience during wakefulness: the state of mind blanking (MB). MB is described as a waking state that is either spontaneous or intentional, during which we do not report any mental content, usually with the feeling of an empty mind[9]. Previous studies have shown that MB is reported about 14-18% of times during focused tasks[9,10] and about 6% of times during resting[11]. The exact nature of mind blanking is still a matter of debate[12,13] and only a few studies have attempted to investigate its neural correlates. Some have reported a widespread deactivation of thalamic and cortical brain regions during spontaneous MB[14] and a more focal deactivation of the superior and inferior frontal gyri and hippocampus during intentional MB, whereas anterior cingulate cortex activation seemed to increase[15]. Others have reported an increase of functional connectivity, as measured by phase coherence metrics, during MB[16]. Finally, MB has been linked to the occurrence of sleep-like slow waves in scalp EEG[8].

Fluctuations of the focus of subjective experience have a measurable impact on behavior and performance. There is extensive literature on the cognitive consequences of MW on sensory

processing, attention, decision making, etc[4]. The behavioral signature of MB is less known. Yet, previous studies revealed a different behavioral profile for MB compared to MW[8]. In the same dataset presented here, while both MW and MB trials were characterized by a similar decrease in accuracy, MW and MB differed in terms of Reaction Times (RTs) and misses (i.e., absence of response when a response is expected) with an acceleration of responses in MW compared to task-focused state, and a deceleration of these responses in MB. These results demonstrate that while MW was characterized by an impulsive behavior (i.e., faster and less accurate responses), MB appeared as a distinct state with more misses and slower RTs than ON and MW, as if they precisely 'blanked' on significant aspects of their current ongoing task.

To date, it still remains unclear whether MW and MB correspond indeed to different subjective and neurophysiological states[17,18] or if they can be traced back to common underlying physiological causes[19]. Recent evidence suggests that both MW and MB could be explained by local sleep phenomena in the brain, but with different regional distributions[8]. Other accounts suggest that MB could arise from a specific pattern of neural (de)activations or functional connectivity, distinguishable from both task-focused and MW states[14,16]. To better understand the true nature of MB in respect to both task-focused and MW states, the neural distinctions of these mind states, if any, need to be further investigated. This investigation should include not only 'resting state' or 'background' brain dynamics, but also neural responses to external stimuli.

Here, we present compelling evidence that MW and MB are indeed two different states, on the phenomenological, behavioral and neurophysiological levels. By capitalizing on the use of neural markers that have been developed to distinguish different conscious or unconscious states[20–22], as well as ERPs[23,24] and time-generalization MVPA techniques[25] allowing to track the processing of external information, we show that MB is characterized by a specific neurophysiological profile that could indeed account for the feeling of absent-mindedness reported at the subjective level as well as the behavioural manifestation of MB.

RESULTS

Behavioral differences between Mind Blanking and Mind Wandering

In this study, 26 healthy participants performed a sustained attention to response task (SART), with digits and faces as stimuli presented in separate blocks, while high-density electro-encephalogram (hdEEG) was recorded continuously. After each stimulus presentation, participants had to press a button (Go trials), or refrain from doing so whenever a “3” or a smiling face was presented (No Go trials; 1 out of 9). Stimulus onset asynchrony (SOA) varied randomly (from 750-1250ms) with a null inter-stimulus interval, and participants’ mental state was probed at random intervals (every 40-70s, uniform random jitter). In particular, participants were instructed to report their attentional focus ‘just before the interruption’ by selecting one of four options: (1) ‘task-focused’ (ON), (2) ‘off-task’ (mind-wandering, MW), (3) ‘mind-blanking’ (MB), or (4) ‘don't remember’. Since the fourth option accounted for only 1.1% of all probes (i.e., less than one probe per participant on average) and given that previous studies did not consistently distinguish between these options[26], we merged third and fourth options as MB in all analyses (Figure 1A-B).

As previously reported[8], participants performed this task with a very high accuracy (mean accuracy of 95 ± 0.1% (SEM)) and with a low rate of Misses (i.e., errors in Go trials, 1.8 ± 0.07). Errors in No Go trials (False alarms) were more frequent (34 ± 0.7%). Nevertheless, participants reported being focused on the task (ON) in only 48 ± 5% of the probes. Concerning the other probes, they mostly reported being in MW (39 ± 4%), and experienced MB in 12 ± 3% of the probes (Figure 1C). Note that the distribution of the ON, MW and MB mind-states was not uniform across participants (see Figure 1C), with large inter-individual differences: in particular 5 participants did not report any MB experience.

In order to detect fine-grained modulations of behavioral performance according to the current participant’s mind-state, we labeled all trials presented up to 20 seconds before each probe as corresponding to the probed state (e.g., after an ‘ON’ response, all previous trials that occurred during the previous 20 seconds were labeled as ‘ON’ trials). As previously reported on the same dataset[8], we found a significant main effect of *mind-state* on accuracy, FA, misses and RTs (see Table 1). Crucially, pairwise comparisons between mind-states revealed that both MW and MB trials were characterized by a similar decrease in accuracy and an increase in FA as compared to ON trials (see Table 1 for details). Yet, we observed opposite modifications concerning RTs: with faster RT for MW as compared to ON, and slower RTs for MB compared to ON trials (and also than MW; see Figure 1D and Table 1). Misses were also

more frequent during MB than during MW and ON states (i.e., MB>MW>ON; see Table 1 and Figure 1D).

'Front-Back' dissociation between Mind Blanking and Mind Wandering

We next investigated neurophysiological correlates of the mind-states (ON, MW and MB) from EEG recorded during the 5s preceding each probe onset. We computed three classes of neural markers: 1) spectral markers (normalized power spectral densities (PSD) in the delta, theta, alpha, beta and gamma bands); 2) complexity markers[21,27] (Kolmogorov Complexity (KC), Approximative Entropy (AE), Sample Entropy (SE) and Permutation Entropy (PE), this last marker being computed in different frequency bands); and 3) connectivity markers *(weighted symbolic mutual information*[20] (wSMI) in the delta, theta, alpha, beta and gamma bands and the *Phase Locking Value* (PLV)). These markers (and other similar measures) have been previously shown to be able to track cognitive and consciousness state modifications in a large range of conditions, including disorders of consciousness (DoC)[20,21,28], sleep[29–31], hypnosis[32] and meditation[33].

A significant main effect of *mind-state*, *electrode location* and of their *interaction* was found for most of the above mentioned neural markers (linear mixed model with mind-state, electrode location and their interaction as main factors, and subject ID as a random intercept; see Table 2). For 3 markers (Kolmogorov complexity, Permutation Entropy in the delta band and PSD gamma), we did not find a main effect of the *mind-state* but we did find a significant interaction effect between the *mind-state* and the *electrode location* (see Table 2). Spectral and complexity measures revealed a diametrically opposite profile between MW and MB: compared to ON, MW was associated both with an increase in fast oscillatory activity and complexity over posterior electrodes, and with a decrease of these metrics over frontal electrodes. A reverse pattern of results was discovered when comparing MB to ON with an increase of fast oscillatory activity and complexity over centro-anterior electrodes, associated with a decrease of these metrics over posterior electrodes. As a logical consequence, the direct comparison between MW and MB showed a front vs. back dissociation: while frontal electrodes showed faster oscillatory activity and higher complexity in MB than in MW, posterior electrodes showed an opposite difference (see Figure 2 panels A and B).

Decreased nonlinear functional connectivity between frontal and posterior regions during Mind Blanking

Functional connectivity analyses revealed a dissociation between the coherence-based metric PLV and the information based metric wSMI. Indeed, while the topographical pattern of the

PLV showed a front vs back dissociation similar to spectral and complexity metrics (with increased values over frontal electrodes and decreased values over posterior electrodes during MB as compared to MW and ON), we observed a progressive breakdown of connectivity from ON to MW, and then from MW to MB for wSMI computed in the alpha, beta and gamma bands, for most electrodes except a few sensors in temporal and occipital regions. In the theta band, the wSMI showed a decrease in both MW and MB as compared to ON, and no significant difference was found in the delta band (see Table 2 and Figure 3 panel A).

To better characterize these connectivity modulations in function of mind state, we reconstructed the cortical sources of the EEG signal (N=68 cortical sources) at the trial level and computed the PLV and the wSMI (at different frequency bands) between each pair of sources (n=2278 connections). These sources were further grouped in 10 pairs (right and left) of 5 ROIs, according to the Desikan-Killiany atlas (frontal, limbic, temporal, parietal and occipital), obtaining thus 45 averaged connections between ROIs. The statistical analysis revealed a main effect of *mind-state* for the PLV and for the wSMI in all frequency bands and an *interaction* effect between *mind-stat*e and the *connection* for the PLV and for all frequency bands of the wSMI except the delta band (linear mixed model with mind-state, connection and their interaction as main factors, and subject ID as a random intercept; see Table 3). As for sensor space analyses, we observed a dissociation between the PLV and the wSMI (see Figure 3 panel B and Figure S1). Regarding the wSMI, the pairwise comparison between MB and MW revealed a breakdown of functional connectivity in MB between frontal areas and posterior associative cortices, within the same frequency bands of interest as reported above in the sensor space. Note that this breakdown affected in particular fronto-parietal connectivity. Both MW and MB showed decreased inter-regional connectivity compared to ON, but the decrease in fronto-posterior connectivity was only present in MB. Interestingly, the PLV showed the opposite pattern, with an increase in functional connectivity between parietal and fronto-temporal areas in MB as compared to ON and MW. As will be discussed later, the contrast between the PLV and wSMI results could reflect the relative implication of linear vs. non-linear interactions between cortical regions during these different mind states, non-linear interactions being best captured by the wSMI (see discussion).

As an interim conclusion, these neurophysiological findings confirmed and extended our behavioral results, by showing that MB is associated with a specific brain state distinct from MW.

Disruption of the late stage of stimulus processing during Mind Blanking

In order to probe the differential neural fate of visual stimuli according to the current mind state, we conducted a single-trial multi-level analysis of event-related potentials (ERPs) (see Methods for details and Table 4 for the results of the statistical model).

Early processing of visual stimuli was extremely similar across ON, MW and MB mind-states. In particular, a similar posterior positivity peaking around 100-150 ms after stimulus presentation, and corresponding to the P1 component[34], was present and identical in all 3 conditions. Crucially, stimulus processing diverged massively as a function of mind-state during the late time-window (>350ms). In ON trials, a classical P3b component (centro-posterior positivity) spanned roughly from 400 to 650 ms after stimulus onset. In MW trials, this P3b pattern was replaced by an anterior positive component from 375 to 700ms. Finally, in this late time-window, amplitudes of MB ERPs were significantly decreased as compared to ON and MW, with no visible P3b or anterior positivity. See Figure 4, panels A and B.

We then computed the cortical sources of the scalp ERP grand-averaged time-series, and tested the activations of these sources as compared to baseline activity. In all conditions, the P1 ERP component was resolved as an early (75ms onset post-stimulus) bilateral occipital activation common to all conditions. The first visible difference between mind states appeared around 150 ms as a brief activation of parietal and frontal cortices that was present in ON and MW trials, but not in MB trials (see Figure 4C). Yet, the most important differences between states appeared during the late time-window starting from 400 ms post stimulus. In both ON and MW conditions, we observed a global cortical activation, involving frontal, parietal, temporal, and occipital cortices. Note however that, during MW, this activation seemed more transient and less extended in space than during ON. Crucially, during MB trials, this late, sustained and widespread pattern boiled down to a very transient activation of left fronto-parieto-occipital cortices, that is contralateral to the side of motor responses.

Taken together scalp and sources results showed the absence of late, sustained and fronto-parietal activation in response to visual stimuli during MB. According to several theories including GNWT[35,36], this new result is highly suggestive of the absence of conscious access to visual stimuli during MB. To further explore this interpretation, we then tested another specific prediction related to conscious access. We tested whether we could decode stimulus type (Faces vs. Digits) from brain responses using a multivariate pattern analysis (MPVA), using the temporal generalization decoding method[25]. Briefly, this analysis consists in training a linear classifier at each time-point to differentiate trials where a Face was presented from trials where a Digit was presented, and then testing its performance at all the other time-points,

thus obtaining a matrix of performance scores for each training/testing time point. These scores track the temporal dynamics and level of processing of mental representations: while an early and "diagonal" pattern of decoding is evocative of a "ballistic" series of successive and transient neural processes, a (usually) late and square-like pattern of decoding is indicative of a sustained neural process, typically encountered in conscious processing[25,32,37]. The classical pattern reported during conscious perception of visual stimuli was present both in ON and MW conditions. Crucially, and as predicted above, the late square-like pattern was clearly disturbed in MB, while the early ballistic diagonal was reduced but still present (see Figure S2).

EEG-based neural features allow for the trial-by-trial prediction of mind state

The exploration of the dynamics of consciousness is limited by the reliance on the discrete sampling of experience through mind probes and subjective reports. To circumvent this snapshot approach, we set out to predict participants' mind-states on a trial-by-trial basis using neural features. We hence computed all of the previously presented EEG markers from stimulus-centered epochs (-0.25 to 0.75 s relative to stimulus onset), for all trials. We then trained and cross-validated, independently for each subject, machine learning classifiers (Random Forest), using exclusively trials within the 5 seconds preceding probe onsets (since we can label these trials as "ground truth" based on subjective reports). Importantly, during the cross-validation procedure, we grouped trials by experimental block to avoid overfitting due to temporal proximity between trials (see Methods for more details). In multiclass classification (ON vs MW vs MB), the median classifier's balanced accuracy score across participants was of 46%, significantly above chance level performance (median chance level (500 permutations): 37%, FDR corrected p-value=0.000009, Wilcoxon rank-sum test, see Methods for more details) (Figure 5A; Table 5).

We then used our trained classifiers to estimate the mind-state in non-labeled trials (>5s before probe onsets). We computed behavioral performance in these trials for each predicted state ($\widehat{ON}$, $\widehat{MW}$, $\widehat{MB}$). Behavioral patterns of predicted states were very similar to the corresponding labeled states: we observed more misses in (predicted) $\widehat{MB}$ trials than in $\widehat{ON}$ and $\widehat{MW}$ trials, as well as longer RTs in $\widehat{MB}$ as compared to $\widehat{MW}$ and $\widehat{ON}$ trials (see Table 6 and Figure 5B). The estimation of the trial-to-trial dynamics between the 3 mind states (transition dynamics, see Figure 6) suggests that, contrary to previous proposals, MB is not a transitory state between MW and ON states. Indeed, the average duration of consecutive sequences of predicted mind states was 7.15 (+/- 0.22) seconds for ON, 2.6 (+/- 0.55) seconds

for MW, and 1.6 (+/-0.21) seconds for MB, revealing that both MB and MW are short-lived mind-states compared to ON-task state (no statistical difference in duration between MW and MB sequences). In addition, the transition matrix further supports this conclusion, by showing that MB trials were as likely to be followed by another MB trial as a MW or ON trial.

DISCUSSION

Mind Blanking corresponds to a specific brain state, different from Mind Wandering

In this study, we examined the behavioral and neural correlates of MB, compared to those of MW and ON states, during a sustained attention task. We showed that MB corresponds to a distinct mental state, characterized by a specific behavioral profile and by specific neural signatures. At a behavioral level, MB had been characterized by response slowing and higher rate of misses, compatible with participants' subjective report of having been "absent minded" during those moments. This behavioral profile was different from the one observed during MW that was characterized by an acceleration of responses and more false alarms, suggestive of an 'impulsive' behavior. At the neural level, both state markers (spectral, complexity and connectivity measures) and brain responses to external stimuli differentiate MB from MW and ON states. A multivariate combination of these neural metrics allowed for the correct prediction of mind-state on a trial-by-trial basis, further supporting the idea that MB, MW and ON states correspond to different mental and neurophysiological states.

These results face the intrinsic problems of the validity and reliability of self-reports during experience sampling[38]. Since we used a probe-catching method where subjective reports were assessed every 1 min or so, we cannot exclude the possibility of mental contents/states happening during the interprobe intervals, and hence missed to be reported. We tried to address this limitation with our classifier's predictions. Finally, our criterion for considering trials as belonging to a particular mind state (20 seconds for behavioral and 5 seconds for EEG analyses) was inspired by previous findings[8] and not data-driven.

Front vs Back dissociation between Mind Blanking and Mind Wandering

We found that spectral and complexity markers display opposite topographical profiles for MW and MB: whereas MW was characterized by decreases of both complexity and fast oscillatory activity over frontal electrodes (compared to ON-task), and by increases of these two EEG metrics over posterior electrodes, MB was associated with a reduction of complexity and fast oscillatory activity over posterior sensors, and with an increase over centro-anterior electrodes. These results are in line with previous analyses in the same dataset[8], that found evidence for sleep-like slow-waves in both MW and MB, but with different regional localizations: while MW was associated with the presence of wake slow-waves over frontal scalp regions, MB was associated with their extension to posterior regions. Two previous fMRI studies showed that spontaneous MB is associated with an extensive cortical and thalamic

de-activation as well as a widespread positive phase-coupling between brain regions[14,16]. Interestingly, chemogenetic inhibition of the mouse prefrontal cortex can result in (i) a decrease in neuronal firing, (ii) the presence of slow oscillations, (iii) an increase in functional connectivity[39], which suggests that the different neural correlates of MB (slow waves, deactivation and hyper-connectivity) could reflect the same neural mechanisms. These results contrast with another study in fMRI focusing this time on voluntary MB, which showed its association with a deactivation of lateral prefrontal regions and hippocampus, but an activation of anterior cingulate cortex[15]. While our spectral and complexity measures were computed in sensor space, and therefore lack precise anatomical information, the observed increase in fast oscillatory activity and neural complexity over centro-anterior electrodes could also be related to ACC activation during MB. Overall these results highlight the necessity to refine the phenomenological characterisation of MB in order to better apprehend its neural correlates[12,13].

Increased phase synchrony with decreased information sharing between frontal and posterior brain regions during Mind Blanking

To date, previous studies have reported mixed results regarding functional connectivity during MB. A previous study using fMRI[15] revealed lower functional connectivity between the default mode network and frontal, visual, and salience networks during voluntary MB as compared to MW. By contrast, using a coherence-based measure, a recent study[16] found a pattern of global positive connectivity (including between frontal and posterior regions) during spontaneous MB. Beyond potential differences between voluntary and spontaneous MB, is important to consider that functional connectivity results depend very much on the type of measure being computed. In the present study, we computed two very different metrics: the PLV[40], a classical coherence-based measure that captures strictly linear correlations, and the wSMI, an information theory based measure which favors non-linear correlations over purely linear ones[20]. While the PLV showed a specific increase of fronto-parietal connectivity in MB as compared to both ON and MW (in line with the previously mentioned study), the wSMI revealed the inverse pattern, with reduced fronto-posterior (and more specifically fronto-parietal) connectivity. Dissociations between coherence-based measures and the wSMI have already been reported, for example when contrasting Wakefulness and N3 sleep, where the whole-brain wSMI was significantly decreased in N3 sleep compared to wakefulness, whereas the wPLI (weighted Phase Lag Index) was not[41]. Our results could reflect a dissociation between increased phase-synchrony with decreased information sharing in MB, which could be caused by the occurrence of synchronous episodes of slow waves and neural silencing over frontal and parietal cortices[42,43], bringing further support to the local sleep hypothesis[8,19]. However, this

dissociation between the PLV and the wSMI connectivity metrics could also be related to higher sensitivity of the PLV to common sources[20,21]. Finally, all our source reconstruction analyses should be interpreted with caution, since this methodology has intrinsic limitations and, additionally, we did not have access to the individual anatomy of each subject.

A lack of conscious access to external information during Mind Blanking?

Stimulus-induced activity analyses (ERPs, source reconstruction and temporal generalization decoding) revealed the preservation of the late (>400ms) and global stage of brain processing of visual stimuli during ON-task and MW trials, whereas this stage of processing was severely disturbed during MB trials.

The neural correlates and signatures of the conscious processing of external information remain highly debated[44,45]. Both theoretical[35,36] and empirical[46–48] work suggest a role of a late (>300ms post-stimulus), sustained and global brain activation, involving in particular fronto-parietal areas, in conscious perception. Previous studies[49–51] have proposed the P3b evoked potential component, the electrophysiological counterpart of this late fronto-parietal activation, as an EEG signature of conscious access. Nevertheless, some authors have claimed that the P3b relates more to post-perceptual processes associated with (external) report than to conscious perception *per se*[52,53]. One elegant way to reconcile all of the above findings was proposed in a recent study[54]. In this study, the authors showed that even in the absence of verbal/motor reports (non-report paradigm[45]), conscious perception is associated with a late, sustained and non-linear brain activation; while the EEG signature of this activation did not correspond to a canonical P3b component, source reconstruction still revealed a broad fronto-parieto-temporal origin. Interestingly, during the active (report) condition, which involves additional decision making processes, additional cortical regions became involved (such as the Supplementary Motor Area), giving rise to a canonical P3b.

Our own results regarding stimulus-induced activity during ON-task and MW mind-states can be interpreted in light of the above findings. Indeed, while the ON-task mind-state can be considered as the equivalent of an active report condition (with all of the attentional and metacognitive ressources being focused on the task), the MW mind-state can be interpreted as a form of non-report condition, with primary perceptual consciousness of the stimulus still existing but without any other form of conscious post-perceptual processing (the motor processes during the SART could be activated unconsciously as is usually the case with simple and repetitive tasks[35,55]). Notably, while the topographies of the evoked components during the late time-window were different between MW and ON-task trials (with a canonical P3b for ON-task and a frontal positive component for MW), source reconstruction still revealed

a late, sustained and broad fronto-parieto-temporal brain activation for both conditions (even if less spatially extended and less sustained during MW, which could be related to the absence of some regions involved in decision making, attentional or metacognitive processes). Crucially, the severe perturbation of this late processing stage in MB trials strongly suggests an absence of conscious perception of visual stimuli during this mind-state. However, the temporal generalization decoding results should be interpreted with caution, since the lack of decoding in the late time window for MB trials could also be related to the significantly lower number of MB trials compared to ON and MW trials.

Probing mind-state without external reports

A multivariate combination of different neural markers could correctly predict the participant's mind state on a trial-by-trial basis. When applying the same classifier to trials away from mind probes and for which we did not have access to specific MW, MB, or ON reports, the fact that we could nonetheless retrieve the behavioral signatures of these states suggests that this MVPA approach captures at least partially the dynamics of conscious experience. Contrary to previous findings[16,26], our results seem to indicate that MB is a genuine brain state, and not only a transitory state between MW and ON states. This proof of concept suggests that we could estimate the second-by-second dynamics of mental states beyond the classical minute-by-minute sampling of subjective experience. This approach paves the way for a fine-grained exploration of the dynamics of consciousness, without under-sampling or interfering with these dynamics by requiring a verbal report.

Conclusion: is Mind Blanking an unconscious state during wakefulness?

Our study provides novel and intriguing insights regarding the state of MB. The impression of an "empty mind" reported by the participants during MB could be accounted for by different mechanisms (i.e., lack of metacognitive awareness, lack of memory encoding, language limitations) other than a lack of conscious experience altogether[13]. Still, several of our results could argue in favor of the more radical interpretation of MB as a "content-free" or even "consciousness-free" mind state. First, various models of consciousness, including the Global Neuronal Workspace Theory[35,36] and Integrated Information Theory[56,57] recognize the posterior associative areas of the brain ("the posterior hot zone") as a key node for the generation of conscious contents. We showed that MB is associated with a significant decrease in neural complexity over the back of the brain. In addition, the Global Neuronal Workspace Theory also posits the sharing of information between posterior (parietal) and frontal areas as key to conscious access. We showed that the fronto-posterior sharing of information as measured by the wSMI was specifically decreased during MB. Finally, while

the presence or absence of internally generated content during MB remains an open question, the severe perturbation of the late stage of processing of visual stimuli during MB trials could argue in favor of a lack of conscious access to external information during this mind state, as already discussed. If MB is indeed a “content free” or even a “consciousness free” state, its existence would challenge our intuition of a continuous conscious experience during wakefulness. In this view, conscious experience would be a discrete phenomenon, with discrete temporal islets of consciousness separated by brief periods of unconsciousness[58]. While puzzling, this perspective would bring even more value to those rare and precious moments of conscious experience.

METHODS

In this work, we used previously collected and published data[8], to answer new research questions.

Experimental procedure and data collection

Participants

A total of thirty-two (N = 32) healthy adult subjects were enrolled in this study. Due to technical complications during the recording process or suboptimal physiological recording quality identified via retrospective visual examination of the data, six individuals were excluded from subsequent analysis. The final study group, comprising 26 participants (age: 29.8 ± 4.1 years, mean ± standard deviation; 10 females), was included in all analyses. Prior to study involvement, participants submitted written informed consent. The Monash University Human Research Ethics Committee granted approval for the study protocol (Project ID: 10994).

Experimental design and stimuli

Participants were positioned in a dimly lit room, seated approximately 60 cm away from a computer screen with their chin supported. Task instructions, stimuli presentation, and button response collection were executed using the Psychtoolbox extension for Matlab (Mathworks, Natick, MA, USA).

The experimental design involved two adapted SARTs, where participants were instructed to focus on a series of human face images during Face SART blocks and on digits during Digit SART blocks. The sequence of Face and Digit blocks was pseudo-randomized for each participant. Each block lasted for roughly 12-15 minutes, with rest periods permitted between blocks. Participants completed three Face SART and three Digit SART blocks, totaling a duration of 103 ± 19.7 minutes (mean ± standard deviation). Prior to each type of Face and Digit SART, participants underwent a brief training session (27 trials) with performance feedback on correct trials and average reaction times (RTs). Participants were urged to prioritize accuracy over speed.

Face and digit stimuli were displayed continuously, with each stimulus shown for 750-1250 ms (uniform random jitter). Face stimuli were derived from the Radboud Face Database, consisting of eight neutral faces (four females, four males) and one smiling female face. Digits ranging from 1 to 9 were displayed in a fixed font size. For Face SART, participants pressed a button for all neutral faces (Go trials) and refrained from pressing the button for the smiling face (No Go trials). The face order was pseudo-randomized throughout the task (presentation

order permuted every nine stimuli, without immediate repetition). For Digit SART, participants pressed a button for all digits except digit 3 (No Go trials), with the digit order pseudo-randomized similarly.

During the SART, stimulus presentation was halted at random intervals (every 40-70 s, uniform random jitter) accompanied by a sound and the word "STOP" on the screen. These interruptions allowed for the assessment of participants' mental states using a series of eight questions. Participants were notably instructed to report their attentional focus "just before the interruption" by selecting one of four options: (1) "task-focused" (ON), (2) "off-task" (mind-wandering, MW), (3) "mind-blanking" (MB), or (4) "don't remember." Since the fourth option accounted for only 1.1% of all probes (less than one probe per participant on average) and previous studies do not consistently distinguish between these options[26], we combined the third and fourth options as MB in all analyses. Participants also rated their vigilance levels over the past few trials on a 4-point scale (1 = Extremely Sleepy, 4 = Extremely Alert). Each 12-15 minute SART block contained ten interruptions (30 interruptions per SART task, 60 interruptions per participant). Participants were briefed on the interruptions and question types prior to the experiment. The mental state categories (ON, MW, and MB) were explained both orally and in writing to participants.

Physiological recordings

High-density scalp EEG data were obtained utilizing an EasyCap with 63 active electrodes, connected to a BrainAmp system (Brain Products GmbH). A ground electrode was positioned frontally (Fpz in the 10-20 system), while electrodes were referenced online to a frontal electrode (AFz). Additional electrodes were placed above and below the left and right canthi to record ocular movements (electrooculogram, EOG). Two electrodes were placed over the deltoid muscles to capture electrocardiographic (ECG) activity. EEG, EOG, and ECG signals were sampled at a rate of 500 Hz. Eye movements and pupil size from one eye were recorded using an EyeLink 1000 system (SR Research) but not analyzed here.

Behavioral analyses

Go trials were deemed incorrect (Miss) if no response was registered between the onset of the stimulus and the subsequent stimulus onset. In contrast, No Go trials were classified as incorrect (false alarm; FA) if a response was detected within the same time frame. Reaction times (RTs) were calculated from the onset of stimulus presentation. Trials with short RTs (<300ms) were discarded and correctness was not determined for these trials. Behavioral performances for each probe were computed using trials within 20 s from probe onset. The

choice of a 20 s window allowed the inclusion of two No Go trials for each probe, while focusing on trials that are relatively close to the probe onset and subsequent subjective reports.

EEG preprocessing and analysis

Preprocessing

Initial preprocessing of the EEG signal was performed in Matlab with a combination of EEGlab and Fieldtrip toolboxes. The raw EEG signal was first high-pass filtered >0.1 Hz using a two-pass fifth-order Butterworth filter. A notch filter was then applied (stopband: [45, 55] Hz, fourth-order Butterworth filter) to remove line noise. Electrodes that were visually identified as noisy throughout the recording were removed and interpolated using neighbouring electrodes. The EEG signal was then decomposed using independent component analysis (ICA), and the components containing ocular artifacts were removed prior to signal reconstruction.

The next steps were performed in Python using the MNE package. The ICA-cleaned EEG signal was down-sampled to 250 Hz, and low-pass filtered <60 Hz. An average reference was applied to all EEG electrodes and the online reference electrode (AFz) was retrieved. Finally, the continuous EEG data were segmented in two different manners, so as to obtain two sets of epochs for different analyses: from -5 to 0 seconds relative to the probe onsets ("Probe epochs"), and from -0.25 to 0.75 seconds relative to the stimuli onsets ("Target epochs"). Probe epochs were labeled according to the mind state reported by the participant at probe onset. Target epochs in the 5 second period prior to the probes were labeled according to the subjective report, all other Target epochs were considered non-labeled (unknown mind state).

Sensor space analyses

Calculation of electroencephalographic markers tracking cognitive modifications

Previous work has shown that cognitive and consciousness state modifications can be tracked using different spectral, complexity or connectivity measures derived from the scalp or intracranial electroencephalographic recording. By combining these markers, it is possible to distinguish conscious participants, patients in a minimal consciousness state and patients with unresponsive wakefulness syndrome[20–22]. These measures can also differentiate sleep stages[29,31,41] and track cognitive and consciousness modifications related to psychedelics or meditation[33]. In our study, we computed these different measures to try to describe the neural correlates of the different mind states (ON, MW and MB). We therefore computed these measures on a trial-by-trial basis on "Probe epochs" (from -5s to 0s relative to probe onsets),

the 5s time-window allowing for both a sufficient time-period for correct maker computation and for (very) close proximity to the subjective reports.

Prior to marker computation, we performed a spatial Laplacian transformation of the EEG signal (also known as Current Source Density (CSD) estimate)[59]. We applied a spherical spline surface Laplacian transformation, with 50 Legendre terms, a stiffness of the spline of value 4 and a regularization parameter (lambda 2) of 1e-5.

Spectral markers

We computed the normalized power spectral densities (PSD) in delta (1-4 Hz), theta (4-8 Hz), alpha (8-12 Hz), beta (12-30 Hz) and gamma (30-60) frequency bands, using Welch's method. The length of each Welch segment (windowed with a Hamming window) was set to be equal to the length of the FFT (fast Fourier transform) and equal to 256 samples (1024 ms). The obtained segments were then averaged, in order to obtain a single value per epoch, channel and frequency. To obtain the normalized PSDs in each frequency band of interest, we: 1) added the raw power of all the frequencies in each frequency band of interest; and 2) computed for each trial and each electrode the normalized PSD by normalizing the raw frequency band PSD by the total power of the electrode.

Complexity markers

We computed four different complexity measures: the Kolmogorov Complexity (KC), the Approximative Entropy (AE), the Sample Entropy (SE) and the Permutation Entropy (PE). While the first three measures are not frequency-specific, PE presents a broad frequency-specific window of sensitivity in function of the value of one the parameters used for its computation (τ). We therefore computed PE in the delta (τ= 64ms), theta (τ= 32ms), alpha (τ= 16ms), beta (τ= 8ms) and gamma (τ= 4ms) bands. Although they differ in their method of calculation, all of these markers measure the level of predictability and regularity of the EEG signal: the more the signal is unpredictable, the more it's algorithmic complexity is important (more information is needed to describe the signal), and the more the complexity of the local neural processing captured by the EEG sensor is assumed to be important.

We computed these four complexity measures for each trial and each EEG electrode (n= 64). See Supplementary material of Sitt et. al (2014)[21] for a detailed description of PE and KC, as well as their computation. Details regarding the AE and SE measures can be found in Richman & Moorman (2000)[27].

Connectivity markers

Weighted symbolic mutual information

We focused on the *weighted symbolic mutual information* (wSMI), a functional connectivity measure capturing linear and non-linear coupling between sensors, which relies on the symbolic transformation of the EEG signal. The wSMI assesses the degree to which two EEG sensors exhibit non-random joint fluctuations, implying information sharing. The time series X and Y in all EEG channels are initially converted into discrete symbol sequences (X^, Y^). These symbols are encoded based on the trends in amplitudes in a predetermined number of consecutive time points. The symbols are therefore defined by two parameters: the number of time points considered (k) and the temporal separation between the time points that constitute a symbol ($\boldsymbol{\tau}$). Following previous work, we chose the parameter k to be 3, implying that the symbols are constituted of three elements, leading to 3! = 6 different potential symbols in total. As for PE, the parameter $\boldsymbol{\tau}$ sets the broad frequency-specific window of sensitivity of this connectivity measure, allowing to compute the wSMI in the delta ($\boldsymbol{\tau}$= 64ms), theta ($\boldsymbol{\tau}$= 32ms), alpha ($\boldsymbol{\tau}$= 16ms), beta ($\boldsymbol{\tau}$= 8ms) and gamma ($\boldsymbol{\tau}$= 4ms) bands. For each frequency band, the joint probability of each pair of symbols co-occurring in two different time series is computed to estimate the *symbolic mutual information* (SMI) shared across two signals. To minimise volume conduction, the *weighted* symbolic mutual information disregards co-occurrences of identical or opposite-sign signals.

The wSMI between two EEG sensors is computed, after symbolic transformation, according to the following formula:

$$\mathrm{wSMI}(\widehat{X},\widehat{Y}) = \frac{1}{log(k!)} \sum\nolimits_{\widehat{x}\epsilon\widehat{X}} \sum\nolimits_{\hat{y}\epsilon\widehat{Y}} w(\widehat{x},\hat{y}) p(\widehat{x},\hat{y}) log \frac{p(\widehat{x},\hat{y})}{p(\widehat{x})p(\hat{y})}$$

where w(x,y) is the weight matrix and p(x,y) is the joint probability of co-occurrence of symbol x in signal X and symbol y in signal Y. Finally p(x) and p(y) are the probabilities of those symbols in each signal.

We computed, in each frequency band, and for each trial, the wSMI between each pair of electrodes (N pairs=2016). To obtain the topographical maps shown in Figure 2, we computed, for each sensor, its median connectivity with all other sensors, obtaining a single value per channel per trial.

Phase Locking Value (PLV)

We also computed a more classical spectral connectivity measure, the Phase Locking Value (PLV), on a trial-by-trial basis. For each channel i, we extracted the instantaneous phase $\phi i^a(t)$ of the analytical signal $xi^a(t)$ of the time series $xi\,(t)$. Then, for each pair (i,j) of channels, we computed the modulus of the time averaged phase difference mapped onto the unit circle:

$$PLV_{ij} = \left| \frac{1}{T} \sum_t e^{i(\phi_i^a(t) - \phi_j^a(t))} \right|$$

As with wSMI, we computed the PLV at trial level for each pair of electrodes, and then we computed the median PLV per EEG channel per trial.

Event related potentials (ERPs) elicited by visual stimuli during the task

In order to study the neural fate of visual stimuli (digits and faces) during the SART task as a function of mind state, we conducted an event related potential analysis on "Target epochs" (-0.25 to 0.75 s relative to stimulus onset). We first applied a baseline correction relative to the -0.25 to 0s time interval. Given the unbalanced nature of our dataset (important variability of the distribution of mind states across participants), we performed a single-trial multi-level analysis of ERPs responses[60] (see Statistics section for more details about this analysis).

Temporal generalization decoding of stimulus type

To further study the neural fate of the visual stimuli as a function of mind state, we assessed whether we could decode stimulus type (Faces vs. Digits) from brain responses using a multivariate pattern analysis (MPVA), with the temporal generalization decoding method[25]. Briefly, this analysis consists in training a linear classifier at each time-point to differentiate trials where a *Face* was presented from trials where a *Digit* was presented, and then testing its performance at all the other time-points (for example,training the classifier at t=2 and testing its ability to correctly classify at t=1,2,3,4,5,…), thus obtaining a whole matrix of performances for each training time point and testing time point. This method provides statistics tracking the temporal dynamics and level of processing of mental representations: while an early and "diagonal" pattern of decoding is evocative of a "ballistic" series of successive and transient neural processes, a (usually) late and square-like pattern of decoding is indicative of a sustained neural process, typically encountered in conscious processing[37] .

Independently for each reported mind state (ON, MW, MB), we standardized the data at the subject level to suppress interindividual variability. At each time sample, and independently

for each channel, channel voltages were standardized across trials sampled from the same participant, by removing the mean and scaling to unit variance. We then trained a linear classifier to decode Digits vs. Faces, using an L2-regularized (C=1) logistic regression, in a 10-fold cross-validation procedure. In each fold, all the trials were shuffled in a pseudo-randomized manner and split into a training set (9/10 of the trials) and a testing set (1/10 of the trials). The classifier's features were the standardized channel amplitudes. This training procedure was applied at each time step independently. Following the time generalization approach, the model trained at each time step was then tested at all the time steps on the testing set trials, at each cross-validation fold. The classifier performance at each training and testing time was evaluated by the area under the receiver operating curve (AUC) at each cross-validation fold. Global performance for each condition and at each training/testing time point was obtained by averaging the AUCs across folds. At each training/testing time point, performance against chance level was computed (see Statistics section).

Decoding of mind-state using dimensionality reduction and a decision tree classifier

Training and testing the classifier on labeled trials

We set out to determine if the participant's mind state could be predicted based on brain activity, on a trial-by-trial basis, using machine learning classifiers. We first focused on "Labeled Target" epochs, where the participant's mind state was considered as known (trials in the 5 seconds before subjective reports). From these epochs, we extracted the previously described EEG metrics (spectral, complexity, and connectivity, see "Calculation of electroencephalographic markers tracking cognitive modifications" section). We also added a supplementary feature, the mean channel voltage during the 0.3-0.5 time period relative to trial onset. For spectral, complexity, and ERP (channel voltages) measures, we extracted for each trial the values of these markers for each EEG channel (obtaining thus 14 x 64 = 896 features). For connectivity markers (wSMI in different frequency bands and the PLV), we used the complete connectivity matrices (2016 connections x 6 metrics = 12,096 features). We hence obtained a total of 12,992 raw features per trial. Given the very high dimensionality of our feature space, we decided to implement a dimensionality reduction technique prior to classification, using a non-linear (kernel) Principal Component Analysis (PCA)[61]. Classification was performed afterwards using Random Forest Classifiers. To take into account individual variability in neural metrics, we trained and tested a PCA/Random Forest classifier independently per participant, the hyperparameters of the PCA (Kernel type, number of components) and of the Random Forest (number of estimators, criterion, maximum depth) being fitted independently for each participant (see below).

To find the best hyperparameters for our PCA/Random Forest pipeline, while also avoiding overfitting, we adopted a “Randomized Grid Search/Cross-validation procedure”, using 200 iterations. We performed this procedure for each participant. In each iteration, a combination of parameter settings was randomly sampled from all specified possible values of each parameter, then the PCA/Random Forest classifier was trained and tested by cross-validation (see below). At the end of all iterations, the set of hyperparameters that obtained the best cross-validated score (balanced accuracy, see below) was selected for further analyses. Comparison to chance level performance was obtained using a 500-permutation procedure, independently for each participant. At each permutation, trial labels were randomly shuffled, then the entire cross-validation procedure was repeated, using the hyperparameters previously selected during the grid search procedure. We thus obtained a distribution of chance-level scores, for each participant. For each participant, we estimated the individual significance against chance by computing a p-value (by counting the number of permutation scores equal or higher to the true score and dividing it by the number of permutations plus one). Group-level significance against chance was also computed, by comparing the distribution of the classifiers' true scores across participants to the distribution of the mean permutation scores across participants (see Statistics section).

Cross-validation was performed using a 5-stratified group fold strategy. In each fold, 4/5 segments of the data were used to train the classifier and the remaining segment was used to test the classifier (computation of the balanced accuracy score, see below). Note that class distributions (proportion of ON, MW, and MB trials) were preserved across partitions of the data. Note also that folds were grouped by experimental block: the blocks that served for the training were not used for the testing. This was done to avoid overfitting linked to temporal proximity of epochs (trials) situated in the same experimental blocks. Note also that this group parameter (experimental block) was also used during the permutation procedure (labels were shuffled inside each block), to avoid over-estimation of significance against chance. At the end of the cross-validation procedure, mean performance scores were obtained by averaging the values obtained in each fold.

We computed a performance score adapted to unbalanced datasets such as ours (unbalanced number of ON, MW, and MB trials): the balanced accuracy score. The balanced accuracy is defined, in multi-class classification, as the average sensitivity Se (“How many relevant items are retrieved?”) for each class. The sensitivity is computed as the number of true positives, divided by the number of true positives plus false negatives. Hence, the balanced accuracy was computed in our dataset according to the following formula:

$$_{Balanced\ accuracy} = \frac{Se_{ON} + Se_{MW} + Se_{MB}}{3}$$
$$= \frac{(TP/TP+FN)_{ON} + (TP/TP+FN)_{MW} + (TP/TP+FN)_{MB}}{3}$$

Note again that all the previously presented steps were performed using the Labeled Target epochs, where the participant's mind state was considered as known (trials in the 5 second period before subjective reports).

Predicting behavioral performances in non-labeled trials

To further test the performances of our classifier, trained on labeled trials, we predicted the mind state in non-labeled trials (more than 5 seconds before probe onsets). To assess the accuracy of this prediction, we once again computed behavioral performances, but this time only on non-labeled trials, and compared the behavioral profile in function of the mind-state in non-labeled trials (according to the classifier's prediction), to the behavioral profile in labeled trials.

Transition dynamics between mind states

We computed the transition probabilities between the different mind states independently for each subject, by counting the total number of transitions between each pair of mind states during inter-probe intervals and normalizing by the total number of occurrences. We then computed the average transition matrices across participants. For this averaging, we only considered subjects that reported having the 3 mind-states (ON, MW and MB). The mind state in non-labeled trials (>5s before probe onsets) was the one predicted by our model, and the mind state in labeled trials (<5s before probe onsets) was the reported mind-state.

Source space analyses

Forward Model and Source Modeling

We used a constrained distributed model consisting of 15,000 current dipoles, constrained to the cortical mantle of a generic brain model obtained from the BrainStorm software package. EEG forward modeling was computed using a symmetric Boundary Element Method (BEM) head model. Current density maps were computed using a minimum norm imaging method[62].

Computation of wSMI and PLV at source level

We estimated the cortical sources of our "Probe epochs". We then extracted trial-to-trial source activity time series of a set of 68 cortical regions, according to a standard anatomical atlas

(Desikan-Killiany[63]). Using the same method described for sensor space analysis, we computed the wSMI and the PLV between each pair of cortical regions (n=2278). Finally, to reduce the number of multiple comparisons and ease the interpretation of this analysis, we computed the median wSMI between pairs of regions of interest (ROIs). To do so, we grouped the 68 cortical regions in 5 pairs of ROIs, according to the Desikan-Killiany atlas (frontal, limbic, temporal, parietal and occipital). The wSMI/PLV between two ROIs was computed as the median across all the connections shared by the two ROIs. We hence computed a wSMI or PLV value for each pair of ROIs (n=45 connections) and each trial, at each frequency band for the wSMI (delta, theta, alpha, beta and gamma).

Source estimation of stimulus evoked activity

For each mind state, we computed at sensor level the average evoked response on “Target epochs” (-0.25 to 0.75s relative to stimuli onsets). The signals were low-pass filtered at 30 Hz. No baseline correction was applied. We then reconstructed the cortical sources of each signal (average evoked response for each mind state) using the methods described above. We finally compared, for each mind state, the stimulus evoked activity to baseline activity (at source level) using a t-test against the baseline period (see Statistics section).

Statistics

Analyses are listed by order of apparition in the results section.

Behaviour

We compared the rate of Misses, FA and the Global Accuracy between mind states at trial level using binomial generalized linear mixed models, with mind state as the explanatory factor and subject ID as a random factor (random intercept). For each behavioral measure and each mind state, response probability and confidence intervals (95%) were back-transformed from the logit scale. For RTs, we used a generalized linear mixed model with mind state as the explanatory factor and subject ID as a random factor (random intercept). To better fit the model assumptions, we applied an inverse transformation (1/RT). Estimated marginal means and confidence intervals (95%) of RTs for each mind state were back-transformed from the inverse scale. All p-values were corrected for multiple comparisons using a Benjamini–Hochberg *False Discovery Rate* (FDR) procedure, with an alpha level at 0.05 (5%) (for n= 32 comparisons) .

Sensor space EEG markers

For each previously described EEG marker, we compared the three mind states (ON, MW, MB) using linear mixed models at trial level, with mind state, EEG sensor (n=64) and their interaction as explanatory factors, and subject ID as a random factor (random intercept). Marker values were standardized (z-scored) across all trials before statistical analysis to better fit the linear mixed models. ANOVA tables were computed from the models. We computed post-hoc contrasts between mind states (model estimates and statistical comparisons) at each EEG sensor. During this post-hoc analysis, to reduce the effect of possibly spurious outliers, we applied a winsorizing procedure to all contrast estimates and uncorrected p-values, were the contrast minima and maxima, as well as the p-value minima were limited to values between -4 and +4 T-values. All p-values were corrected for multiple comparisons using an FDR procedure. Main factor's p-values were corrected across the number of factors and the number of EEG markers (n_factors x n_markers= 3x18= 54 comparisons, alpha level = 0.05). Post-hoc p-values for each EEG marker were corrected after winsorization across the number of EEG sensors and the number of conditions (correction for n_sensors x n_conditions= 64 x 3=192 comparisons, alpha level = 0.05) .

Source space wSMI

For each frequency band, we performed a linear mixed model at trial level, with mind state, connection id (ROI1-ROI2) (n=45) and their interaction as explanatory factors, and subject ID as a random factor (random intercept). As before, we computed ANOVA tables and post-hoc contrasts between mind-states for each pair of source ROIs, correcting all p-values for multiple comparisons using an FDR procedure, as described above.

Sensor space ERPs

We performed a mass-univariate (across time and space dimensions) single-trial multi-level analysis of ERPs responses. We initially intended to add both *EEG channel* and *time* (in addition to *mind state*) as factors to the same mixed linear model, but this was not feasible for computational reasons. We therefore subsampled our time dimension (-250 to 750 ms relative to stimuli onsets) by using a -25 to +25ms sliding time-window, with 75ms steps, resulting in a set of 10 time-windows of interest. We then performed a linear mixed model for each time-window, with *channel amplitude* as the dependent factor; *mind state*, *EEG sensor* and their interaction as explanatory factors; and subject ID as a random factor (random intercept). For each time-window, voltage estimates for each mind state, and their statistical comparisons, were computed for each EEG sensor. All obtained p-values were corrected for multiple

comparisons using an FDR procedure (for n_sensors x n_conditions x n_times = 64 x 3 x 10 = 1920 comparisons, alpha level = 0.05).

Temporal generalization decoding

For each mind-state, classification performance at each training and testing time was tested against 0.5 (chance) using a two-sided non-parametric sign test across validation folds, and these statistics were then corrected for multiple comparisons using an FDR procedure (for n_times x n_times= 63 001 comparisons, alpha level = 0.05).

Source estimation of stimulus evoked activity

We performed a t-test against baseline at each time sample and each cortical source, and corrected for multiple comparisons across time, space and frequency dimensions using an FDR procedure (alpha=0.05).

Comparison to chance level performance of the classifier trained to distinguish different mind states

As already explained in the previous sections, we compared our classifiers' performances to chance level using a 500-permutation procedure. We performed this procedure for each participant. At each permutation, trial labels were randomly shuffled (grouped by experimental blocks), then the entire training/testing cross-validation procedure was repeated, using the hyperparameters previously selected during the grid search procedure. We thus obtained a distribution of chance-level scores, for each participant. To calculate the individual p-value, we counted the number of permutation scores equal or higher to our true score and divided it by the number of permutations plus one. To assess group level statistical significance against chance, we performed a two-tailed Wilcoxon rank sum test, where we compared the distribution of true classification scores across participants (non permuted data), to the distribution of mean permutation scores (permuted data) across participants.

Software

Most analyses were performed in Python 3.9.13 , using the following packages:

- MNE (v 1.4.2) (https://mne.tools/stable/index.html): preprocessing and manipulation of EEG data
- MNE-features (v 0.2.1) (https://mne.tools/mne-features/) and nice-tools (https://github.com/nice-tools/nice): computation of EEG neural markers

- Pymer4 (v 0.8.0) (https://eshinjolly.com/pymer4/) and pingouin (v 0.5.3) (https://pingouin-stats.org/build/html/index.html) : statistical analysis
- Scikit-learn (v 1.3) (https://scikit-learn.org/stable/) : machine learning analyses

Binomial mixed models (for behavioral analyses) were performed in R using the *lme4* and *emmeans* libraries.

Source reconstruction analyses were performed in Matlab using the Brainstorm package (https://neuroimage.usc.edu/brainstorm/Introduction)

Initial preprocessing of raw EEG files using ICA was performed in Matlab using EEGlab 2021.1 and FieldTrip-20210807.

REFERENCES

1. James, W. *The Principles of Psychology*. (Henry Holt and Company, New York, 1890).

2. Chun, M. M., Golomb, J. D. & Turk-Browne, N. B. A Taxonomy of External and Internal Attention. *Annual Review of Psychology* **62**, 73–101 (2011).

3. Smallwood, J., Obonsawin, M. & Heim, D. Task unrelated thought: the role of distributed processing. *Conscious Cogn* **12**, 169–189 (2003).

4. Smallwood, J. & Schooler, J. W. The Science of Mind Wandering: Empirically Navigating the Stream of Consciousness. *Annual Review of Psychology* **66**, 487–518 (2015).

5. Gruberger, M., Simon, E., Levkovitz, Y., Zangen, A. & Hendler, T. Towards a Neuroscience of Mind-Wandering. *Frontiers in Human Neuroscience* **5**, (2011).

6. Compton, R. J., Gearinger, D. & Wild, H. The wandering mind oscillates: EEG alpha power is enhanced during moments of mind-wandering. *Cogn Affect Behav Neurosci* **19**, 1184–1191 (2019).

7. Braboszcz, C. & Delorme, A. Lost in thoughts: neural markers of low alertness during mind wandering. *Neuroimage* **54**, 3040–3047 (2011).

8. Andrillon, T., Burns, A., Mackay, T., Windt, J. & Tsuchiya, N. Predicting lapses of attention with sleep-like slow waves. *Nat Commun* **12**, 3657 (2021).

9. Ward, A. & Wegner, D. Mind-blanking: when the mind goes away. *Frontiers in Psychology* **4**, (2013).

10. Schooler, J. W., Reichle, E. D. & Halpern, D. V. Zoning Out while Reading: Evidence for Dissociations between Experience and Metaconsciousness. in *Thinking and seeing: Visual metacognition in adults and children* 203–226 (MIT Press, Cambridge, MA, US, 2004).

11. Van Calster, L., D'Argembeau, A., Salmon, E., Peters, F. & Majerus, S. Fluctuations of Attentional Networks and Default Mode Network during the Resting State Reflect Variations in Cognitive States: Evidence from a Novel Resting-state Experience Sampling Method. *Journal of Cognitive Neuroscience* **29**, 95–113 (2017).

12. Kaufmann, A., Parmigiani, S., Kawagoe, T., Zabaroff, E. & Wells, B. Two models of mind blanking. *Eur J of Neuroscience* ejn.16164 (2023) doi:10.1111/ejn.16164.

13. Fell, J. What is mind blanking: A conceptual clarification. *Eur J of Neuroscience* **56**, 4837–4842 (2022).

14. Boulakis, P. A., Mortaheb, S., Van Calster, L., Majerus, S. & Demertzi, A. Whole-Brain Deactivations Precede Uninduced Mind-Blanking Reports. *J. Neurosci.* **43**, 6807–6815 (2023).

15. Kawagoe, T., Onoda, K. & Yamaguchi, S. The neural correlates of "mind blanking": When the mind goes away. *Human Brain Mapping* **40**, 4934–4940 (2019).

16. Mortaheb, S. *et al.* Mind blanking is a distinct mental state linked to a recurrent brain profile of globally positive connectivity during ongoing mentation. *Proceedings of the National Academy of Sciences* **119**, e2200511119 (2022).

17. Mittner, M., Hawkins, G. E., Boekel, W. & Forstmann, B. U. A Neural Model of Mind Wandering. *Trends in Cognitive Sciences* **20**, 570–578 (2016).

18. Unsworth, N. & Robison, M. K. Tracking arousal state and mind wandering with pupillometry. *Cogn Affect Behav Neurosci* **18**, 638–664 (2018).

19. Andrillon, T. *et al.* Does the Mind Wander When the Brain Takes a Break? Local Sleep in Wakefulness, Attentional Lapses and Mind-Wandering. *Frontiers in Neuroscience* **13**, (2019).

20. King, J.-R. *et al.* Information Sharing in the Brain Indexes Consciousness in Noncommunicative Patients. *Current Biology* **23**, 1914–1919 (2013).

21. Sitt, J. D. *et al.* Large scale screening of neural signatures of consciousness in patients in a vegetative or minimally conscious state. *Brain* **137**, 2258–2270 (2014).

22. Engemann, D. A. *et al.* Robust EEG-based cross-site and cross-protocol classification of states of consciousness. *Brain* **141**, 3179–3192 (2018).

23. Luck, S. J., Woodman, G. F. & Vogel, E. K. Event-related potential studies of attention. *Trends in Cognitive Sciences* **4**, 432–440 (2000).

24. Dehaene, S. *et al.* Imaging unconscious semantic priming. *Nature* **395**, 597–600 (1998).

25. King, J.-R. & Dehaene, S. Characterizing the dynamics of mental representations: the temporal generalization method. *Trends in Cognitive Sciences* **18**, 203–210 (2014).

26. Van den Driessche, C. *et al.* Attentional Lapses in Attention-Deficit/Hyperactivity Disorder: Blank Rather Than Wandering Thoughts. *Psychol Sci* **28**, 1375–1386 (2017).

27. Richman, J. S. & Moorman, J. R. Physiological time-series analysis using approximate entropy and sample entropy. *American Journal of Physiology-Heart and Circulatory Physiology* **278**, H2039–H2049 (2000).

28. Engemann, D. A. *et al.* Robust EEG-based cross-site and cross-protocol classification of states of consciousness. *Brain* **141**, 3179–3192 (2018).

29. Bourdillon, P. *et al.* Brain-scale cortico-cortical functional connectivity in the delta-theta band is a robust signature of conscious states: an intracranial and scalp EEG study. *Scientific Reports* **10**, 1–13 (2020).

30. Schartner, M. M. *et al.* Global and local complexity of intracranial EEG decreases during NREM sleep. *Neuroscience of Consciousness* **2017**, (2017).

31. Türker, B. *et al.* Behavioral and brain responses to verbal stimuli reveal transient periods of cognitive integration of external world in all sleep stages. 2022.05.04.490484 Preprint at https://doi.org/10.1101/2022.05.04.490484 (2022).

32. Munoz Musat, E., Rohaut, B., Sangare, A., Benhaiem, J.-M. & Naccache, L. Hypnotic Induction of Deafness to Elementary Sounds: An Electroencephalography Case-Study and a Proposed Cognitive and Neural Scenario. *Frontiers in Neuroscience* **16**, (2022).

33. Martínez Vivot, R., Pallavicini, C., Zamberlan, F., Vigo, D. & Tagliazucchi, E. Meditation Increases the Entropy of Brain Oscillatory Activity. *Neuroscience* **431**, 40–51 (2020).

34. Spehlmann, R. The averaged electrical responses to diffuse and to patterned light in the human. *Electroencephalogr Clin Neurophysiol* **19**, 560–569 (1965).

35. Dehaene, S. Towards a cognitive neuroscience of consciousness: basic evidence and a workspace framework. *Cognition* **79**, 1–37 (2001).

36. Mashour, G. A., Roelfsema, P., Changeux, J.-P. & Dehaene, S. Conscious Processing and the Global Neuronal Workspace Hypothesis. *Neuron* **105**, 776–798 (2020).

37. Sanchez, G., Hartmann, T., Fuscà, M., Demarchi, G. & Weisz, N. Decoding across sensory modalities reveals common supramodal signatures of conscious perception. *PNAS* **117**, 7437–7446 (2020).

38. Nisbett, R. E. & Wilson, T. D. Telling more than we can know: Verbal reports on mental processes. *Psychological Review* **84**, 231–259 (1977).

39. Rocchi, F. *et al.* Increased fMRI connectivity upon chemogenetic inhibition of the mouse prefrontal cortex. *Nat Commun* **13**, 1056 (2022).

40. Aydore, S., Pantazis, D. & Leahy, R. M. A note on the phase locking value and its properties. *NeuroImage* **74**, 231–244 (2013).

41. Imperatori, L. S. *et al.* EEG functional connectivity metrics wPLI and wSMI account for distinct types of brain functional interactions. *Sci Rep* **9**, 8894 (2019).

42. Aedo-Jury, F., Schwalm, M., Hamzehpour, L. & Stroh, A. Brain states govern the spatio-temporal dynamics of resting-state functional connectivity. *eLife* **9**, e53186 (2020).

43. El-Baba, M. *et al.* Functional connectivity dynamics slow with descent from wakefulness to sleep. *PLOS ONE* **14**, e0224669 (2019).

44. Aru, J., Bachmann, T., Singer, W. & Melloni, L. Distilling the neural correlates of consciousness. *Neuroscience & Biobehavioral Reviews* **36**, 737–746 (2012).

45. Tsuchiya, N., Wilke, M., Frässle, S. & Lamme, V. A. F. No-Report Paradigms: Extracting the True Neural Correlates of Consciousness. *Trends in Cognitive Sciences* **19**, 757–770 (2015).

46. Dehaene, S. *et al.* Cerebral mechanisms of word masking and unconscious repetition priming. *Nat. Neurosci.* **4**, 752–758 (2001).

47. Gaillard, R. *et al.* Converging Intracranial Markers of Conscious Access. *PLoS Biol* **7**, (2009).

48. Vuilleumier, P. *et al.* Neural fate of seen and unseen faces in visuospatial neglect: A combined event-related functional MRI and event-related potential study. *Proc Natl Acad Sci U S A* **98**, 3495–3500 (2001).

49. Sergent, C., Baillet, S. & Dehaene, S. Timing of the brain events underlying access to consciousness during the attentional blink. *Nature Neuroscience* **8**, 1391–1400 (2005).

50. Del Cul, A., Baillet, S. & Dehaene, S. Brain Dynamics Underlying the Nonlinear Threshold for Access to Consciousness. *PLoS Biol* **5**, (2007).

51. Bekinschtein, T. A. *et al.* Neural signature of the conscious processing of auditory regularities. *PNAS* **106**, 1672–1677 (2009).

52. Cohen, M. A., Ortego, K., Kyroudis, A. & Pitts, M. Distinguishing the Neural Correlates of Perceptual Awareness and Postperceptual Processing. *J. Neurosci.* **40**, 4925–4935 (2020).

53. Pitts, M. A., Metzler, S. & Hillyard, S. A. Isolating neural correlates of conscious perception from neural correlates of reporting one's perception. *Front Psychol* **5**, 1078 (2014).

54. Sergent, C. *et al.* Bifurcation in brain dynamics reveals a signature of conscious processing independent of report. *Nat Commun* **12**, 1149 (2021).

55. Dehaene, S. *et al.* Imaging unconscious semantic priming. *Nature* **395**, 597–600 (1998).

56. Tononi, G. The Integrated Information Theory of Consciousness: An Updated Account. *Archives Italiennes de Biologie* **150**, 56–90 (2012).

57. Oizumi, M., Albantakis, L. & Tononi, G. From the Phenomenology to the Mechanisms of Consciousness: Integrated Information Theory 3.0. *PLoS Computational Biology* **10**, e1003588 (2014).

58. Naccache, L. Why and how access consciousness can account for phenomenal consciousness. *Philosophical Transactions of the Royal Society B: Biological Sciences* **373**, 20170357 (2018).

59. Kayser, J. & Tenke, C. E. Principal components analysis of Laplacian waveforms as a generic method for identifying ERP generator patterns: II. Adequacy of low-density estimates. *Clinical Neurophysiology* **117**, 369–380 (2006).

60. Volpert-Esmond, H. I., Merkle, E. C., Levsen, M. P., Ito, T. A. & Bartholow, B. D. Using Trial-Level Data and Multilevel Modeling to Investigate Within-Task Change in Event-Related Potentials. *Psychophysiology* **55**, e13044 (2018).

61. Weston, J., Schölkopf, B. & Bakir, G. Learning to Find Pre-Images. in *Advances in Neural Information Processing Systems* vol. 16 (MIT Press, 2003).

62. Baillet, S., Mosher, J. C. & Leahy, R. M. Electromagnetic brain mapping. *IEEE Signal Processing Magazine* **18**, 14–30 (2001).

63. Desikan, R. S. *et al.* An automated labeling system for subdividing the human cerebral cortex on MRI scans into gyral based regions of interest. *NeuroImage* **31**, 968–980 (2006).

Acknowledgments:

We thank Teigane Mackay for data collection, Naotsugu Tsuchiya, and Jennifer Windt for their support to TA at the inception of this line of research, and Jakob Howhy, Delphine Oudiette and Jacobo Sitt for the discussion about the nature and dynamics of consciousness. AWC acknowledges the support of the Three Springs Foundation.

Funding:

Agence Nationale de la Recherche ANR-22-CE37–0006-01 (TA)

Human Frontiers Science Program LT000362/2018-L (TA)

Author contributions:

Conceptualization: EMM, AWC, LN, TA

Methodology: EMM, AWC, LB, LN, TA

Investigation: EMM, TA

Visualization: EMM, TA

Funding acquisition: LN, TA

Supervision: LN, TA

Writing – original draft: EMM

Writing – review & editing: EMM, AWC, LN, TA

Competing interests:

Authors declare that they have no competing interests.

Data and materials availability:

All data, code, and materials used in the analysis will be freely available upon publication.

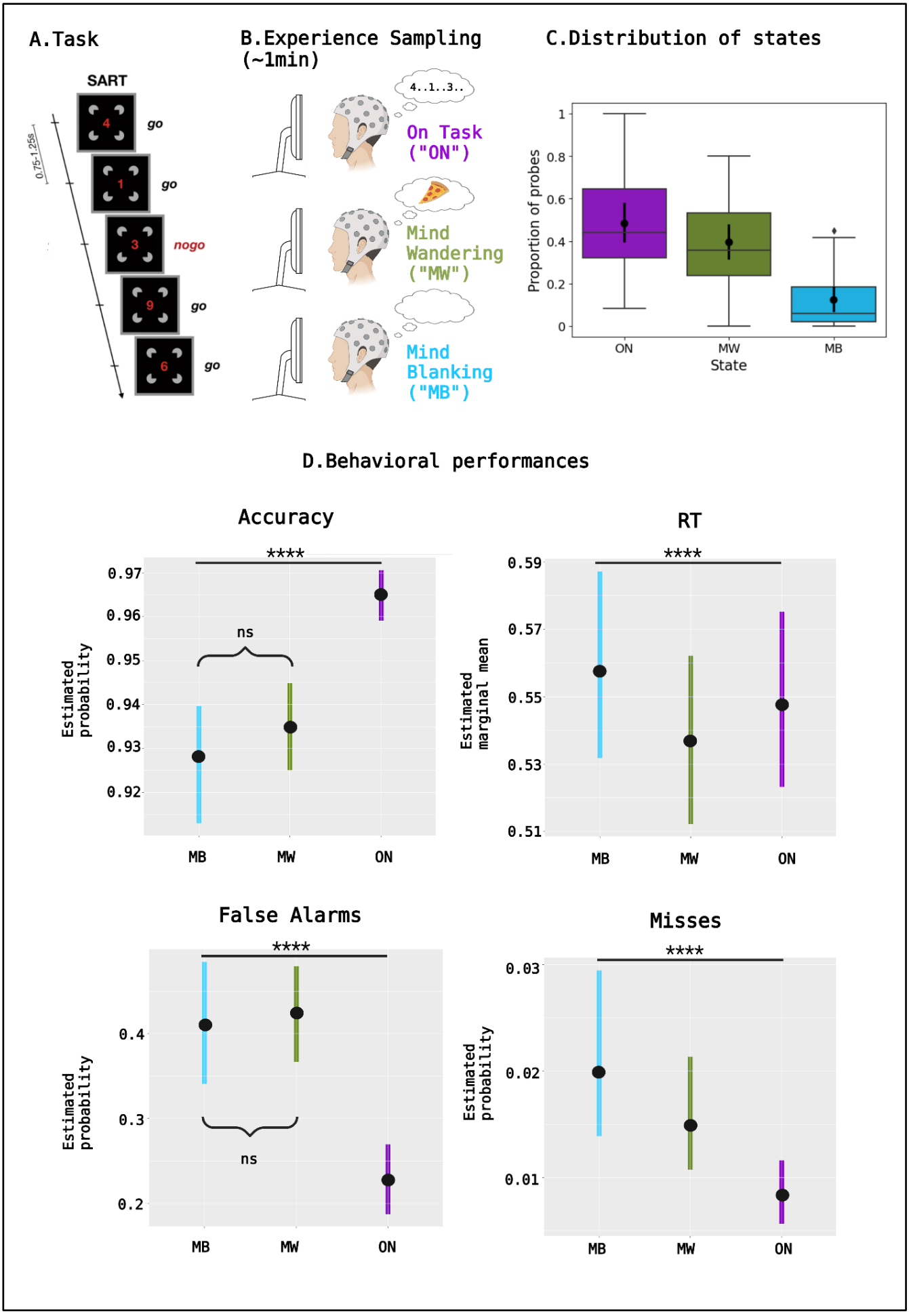
A.Task
SART
0.75-1.25s
go
go
nogo
go
go
B.Experience Sampling (~1min)
4..1..3..
On Task ("ON")
Mind Wandering ("MW")
Mind Blanking ("MB")
C.Distribution of states
Proportion of probes
ON
MW
MB
State
D.Behavioral performances
Accuracy
Estimated probability
****
ns
MB
MW
ON
RT
Estimated marginal mean
****
MB
MW
ON
False Alarms
Estimated probability
****
ns
MB
MW
ON
Misses
Estimated probability
****
MB
MW
ON

Figure 1: Experimental paradigm and behavioral results. Panels A and B: Experimental paradigm. 26 healthy participants performed a sustained attention to response task (SART), with digits and faces as stimuli, while high-density electro-encephalogram (EEG) was recorded continuously. After each stimulus presentation, participants had to press a button (Go trials), or refrain from doing so, whenever a "3" or a smiling face was presented (No Go trials; 1 out of 9). SOA varied randomly (750-1250ms) with a null ISI (panel A). Participants' mental state was probed at random intervals (every 40-70s, uniform random jitter). They had to report their attentional focus by selecting one of four options: (1) 'task-focused' (ON), (2) 'off-task' (mind-wandering, MW), (3) 'mind-blanking' (MB) (panel B). Panel C: proportion of probes in function of the reported mind-state. Proportions were computed at subject level and the distributions at group level are represented by a boxplot (the boundaries of the boxes represent first and third quartiles (Q1 and Q3 respectively), mid-line represents the medium and the whiskers depict Q1-1.5*IQR and Q3*1.5*IQR) and by a mean-plot (mean +/- IC95%). Panel D: Behavioral performances in function of the reported mind-state. Accuracy, response times (RT), False Alarms and Misses were computed for the trials between the 20s before probe-onsets. (Binomial) linear mixed models were computed with *mind-state* as the main explanatory factor, and subject ID as a random intercept. We found fine-grained modulations of performance in function of mind-state, with distinct behavioral profiles for MW (faster RTs) and MB (slower RTs, more misses). The statistical bar and stars represent the main effect of mind-state, and all pairwise comparisons between states are statistically significant unless otherwise signaled (n.s.). The detailed statistical results can be found on Table 1.

****: FDR corrected p-value<0.0001

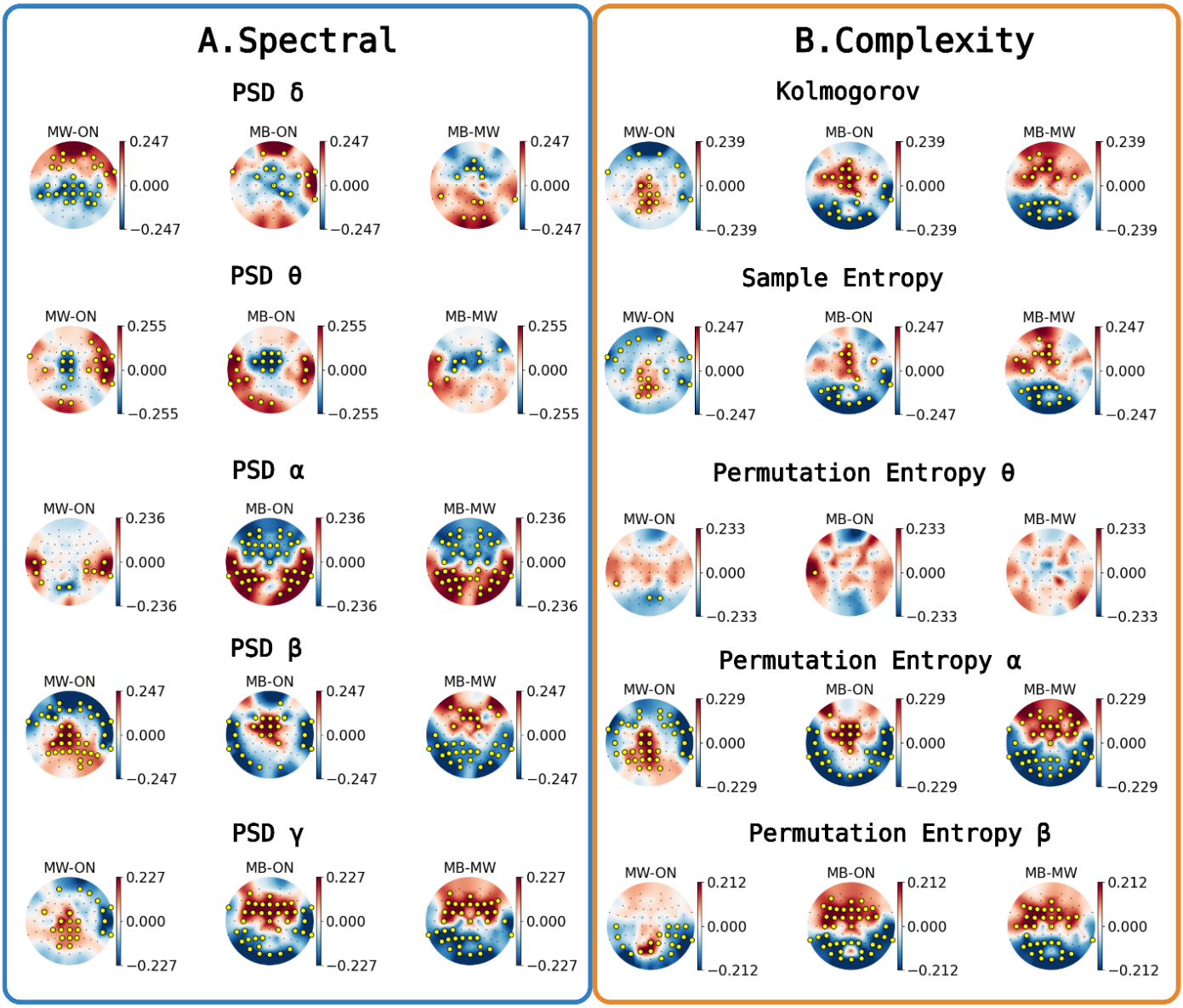
A.Spectral
PSD δ
MW-ON
0.247
0.000
−0.247
MB-ON
0.247
0.000
−0.247
MB-MW
0.247
0.000
−0.247
PSD θ
MW-ON
0.255
0.000
−0.255
MB-ON
0.255
0.000
−0.255
MB-MW
0.255
0.000
−0.255
PSD α
MW-ON
0.236
0.000
−0.236
MB-ON
0.236
0.000
−0.236
MB-MW
0.236
0.000
−0.236
PSD β
MW-ON
0.247
0.000
−0.247
MB-ON
0.247
0.000
−0.247
MB-MW
0.247
0.000
−0.247
PSD γ
MW-ON
0.227
0.000
−0.227
MB-ON
0.227
0.000
−0.227
MB-MW
0.227
0.000
−0.227
B.Complexity
Kolmogorov
MW-ON
0.239
0.000
−0.239
MB-ON
0.239
0.000
−0.239
MB-MW
0.239
0.000
−0.239
Sample Entropy
MW-ON
0.247
0.000
−0.247
MB-ON
0.247
0.000
−0.247
MB-MW
0.247
0.000
−0.247
Permutation Entropy θ
MW-ON
0.233
0.000
−0.233
MB-ON
0.233
0.000
−0.233
MB-MW
0.233
0.000
−0.233
Permutation Entropy α
MW-ON
0.229
0.000
−0.229
MB-ON
0.229
0.000
−0.229
MB-MW
0.229
0.000
−0.229
Permutation Entropy β
MW-ON
0.212
0.000
−0.212
MB-ON
0.212
0.000
−0.212
MB-MW
0.212
0.000
−0.212

Figure 2: EEG-based neurophysiological markers differentiate MB from ON and MW. Spectral (A) and Complexity (B) results. Each subplot represents the pairwise statistical contrast between two states (left: MW - ON; middle: MB - ON; right: MB - MW), at sensor level (topographical representation of the scalp). Model estimates for the contrast between states were computed for each electrode, and locations with statistically significant differences (FDR corrected p-value<0.05) are depicted with a golden circle. We observed a front-back dissociation between MW and MB for spectral and complexity measures. The ANOVA tables summarizing the main factor's effects (linear mixed models with mind-state, electrode/connection and their interaction as main factors, and subject ID as a random intercept) for each EEG metric can be found in Table 2.

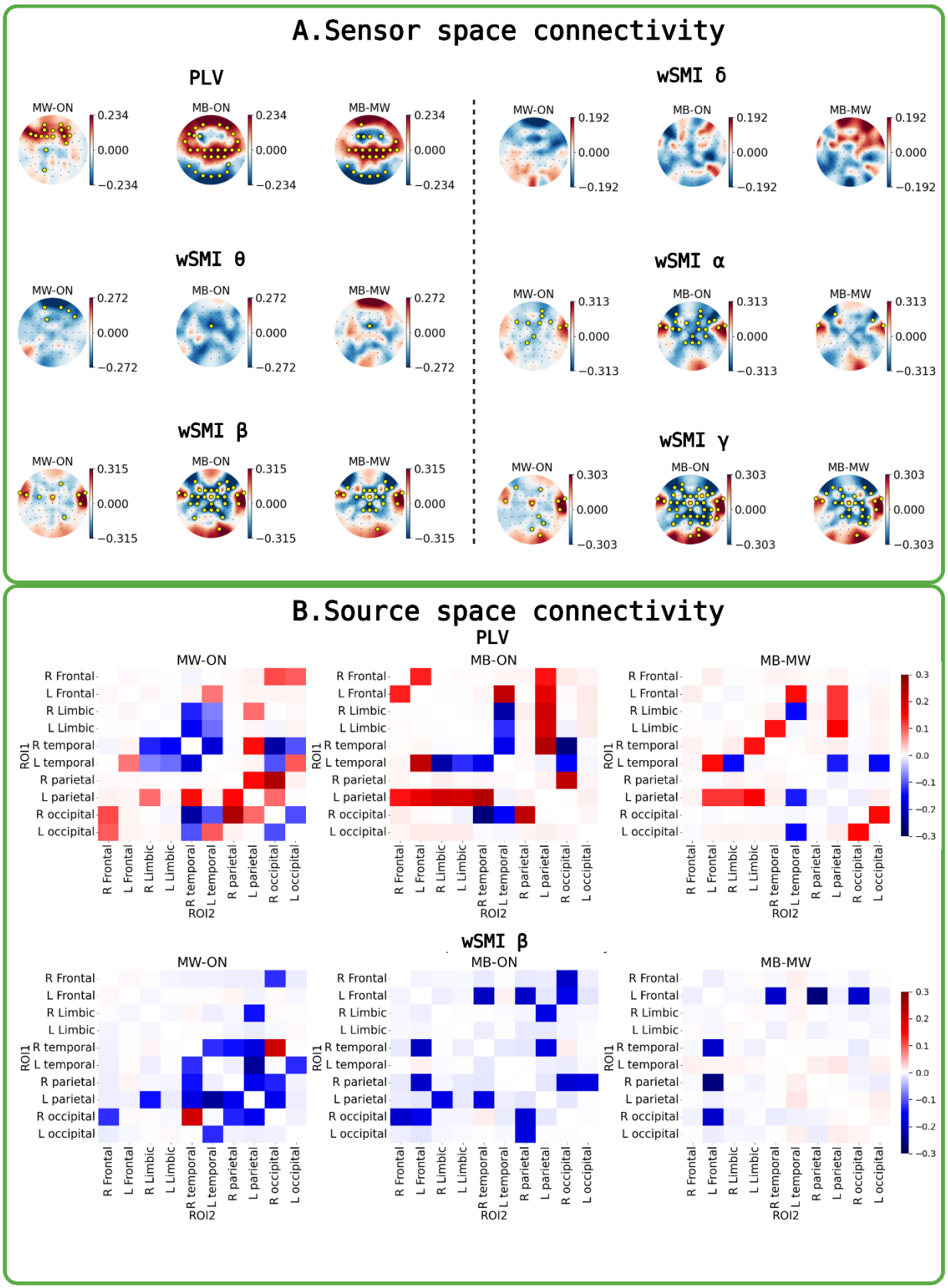
A.Sensor space connectivity
PLV
wSMI δ
wSMI θ
wSMI α
wSMI β
wSMI γ
MW-ON
MB-ON
MB-MW
0.234
0.000
−0.234
0.192
−0.192
0.272
−0.272
0.313
−0.313
0.315
−0.315
0.303
−0.303
B.Source space connectivity
PLV
wSMI β
ROI1
ROI2
R Frontal
L Frontal
R Limbic
L Limbic
R temporal
L temporal
R parietal
L parietal
R occipital
L occipital

Figure 3: Increased phase synchrony with reduced information sharing during MB. Sensor space (A) and source space (B) connectivity results. **(A):** Each subplot represents the pairwise statistical contrast between two states (left: MW - ON; middle: MB - ON; right: MB - MW), at sensor level (topographical representation of the scalp). Model estimates for the contrast between states were computed for each electrode, and locations with statistically significant differences (FDR corrected p-value<0.05) are depicted with a golden circle. The ANOVA tables summarizing the main factor's effects (linear mixed models with mind-state, electrode/connection and their interaction as main factors, and subject ID as a random intercept) for each EEG metric can be found in Table 2. We observed a dissociation between the PLV and wSMI metrics, with an increase of the PLV over frontal electrodes and a decrease over posterior electrodes during MB, while the wSMI was globally decreased during MB. **(B):** PLV (top) and wSMI in the beta band (bottom) computed at the source level. Each square-matrix represents the contrast in connectivity, computed in source space, between two mind-states, for each pair of regions of interest (ROIs). Only significantly different connections (FDR corrected p-value<0.05) are highlighted, the other ones are masked. ANOVA tables for the statistical models can be found in Table 3. The wSMI at source level for other frequency bands can be found in Figure S1. We observed a dissociation between the PLV and wSMI, with increased PLV (phase synchrony) and decreased wSMI (information sharing) between frontal and parietal/posterior regions during MB, as compared to ON and MW.

δ: delta band; θ: theta band; α: alpha band; β: beta band; γ: gamma band
wSMI: weighted symbolic mutual information
PLV: Phase Locking Value
R: right; L: left

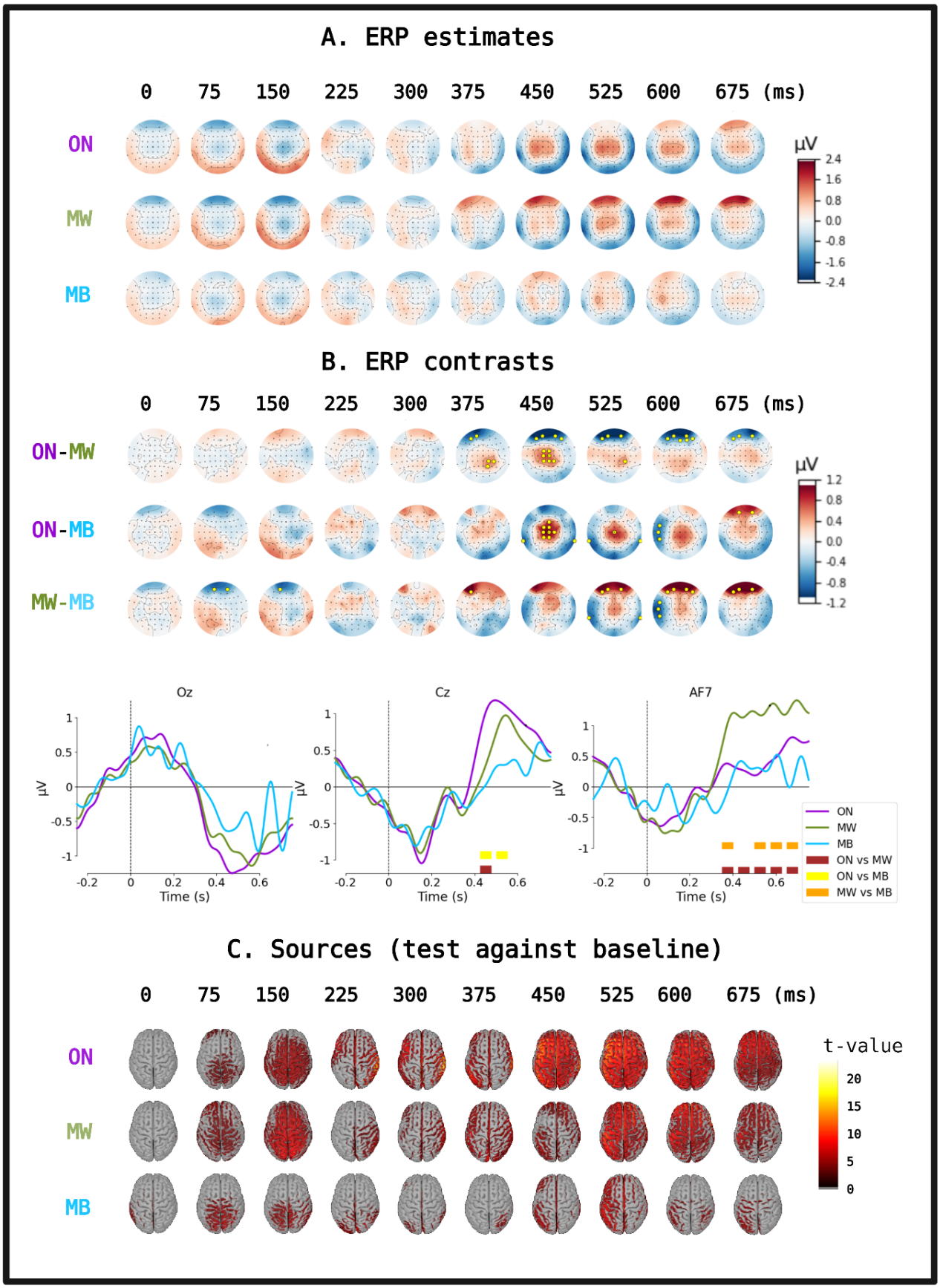
A. ERP estimates
0 75 150 225 300 375 450 525 600 675 (ms)
ON
MW
MB
µV
2.4
1.6
0.8
0.0
-0.8
-1.6
-2.4
B. ERP contrasts
0 75 150 225 300 375 450 525 600 675 (ms)
ON-MW
ON-MB
MW-MB
µV
1.2
0.8
0.4
0.0
-0.4
-0.8
-1.2
Oz
Cz
AF7
µV
Time (s)
ON
MW
MB
ON vs MW
ON vs MB
MW vs MB
C. Sources (test against baseline)
0 75 150 225 300 375 450 525 600 675 (ms)
ON
MW
MB
t-value
20
15
10
5
0

Figure 4: Event related potentials (ERPs). Panels A and B: Topographical scalp representation of the ERP estimates for each mind state (A) and ERP contrasts between mind-states (B), derived from the statistical model (single-trial multi-level analysis with mind-state, EEG channel and their interaction as main factors, and subject ID as a random intercept). Marked electrodes in panel B (golden circles) are the ones presenting a statistically significant difference between conditions (FDR corrected p-value<0.05). Panel B bottom presents the grand-average ERP time-series for each mind-state (ON: violet; MW: green; MB: blue) for 3 electrodes of interest (Oz, Cz and AF7). Time-points with statistically significant differences between conditions (FDR corrected p-value<0.05) are highlighted (ON vs MW: brown; ON vs MB: yellow; MW vs MB: orange). Panel C: Source reconstruction of the grand-average ERP for each mind-state. A t-test against the baseline (-0.25 to 0s relative to stimulus onset) was performed, and only statistically significant activations compared to the baseline (FDR corrected p-value<0.05, corrected for multiple comparisons across time, space and frequencies) are highlighted. Both sensor space and source space ERPs results showed differences between mind-states mainly in the late time-window (>400ms), with a significant decrease of late evoked activity in MB trials compared to MW and ON trials.

A. 500-permutation test results of the PCA/RF classifier (trained and tested by cross-validation on labeled trials)

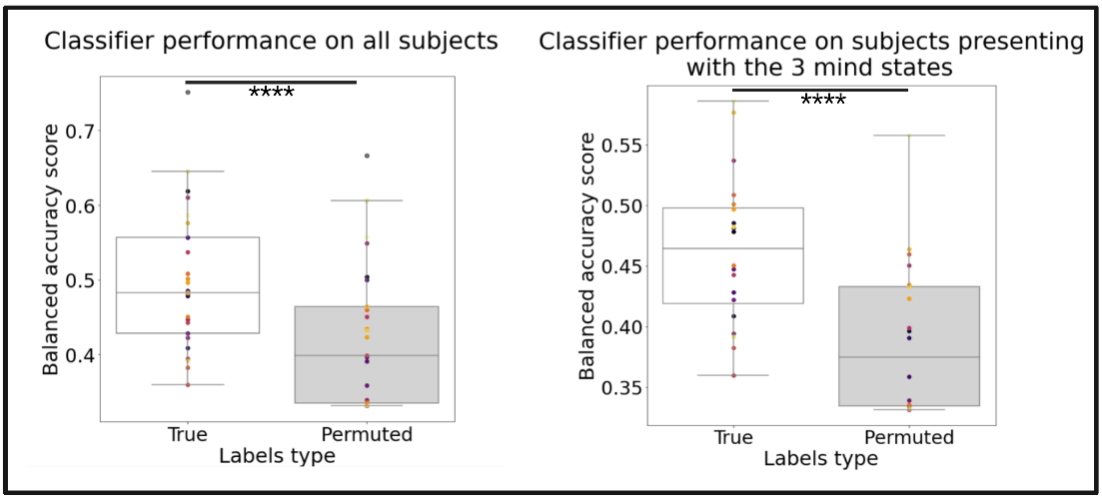

B. Behavioral performances in function of the predicted mind state in non-labeled trials

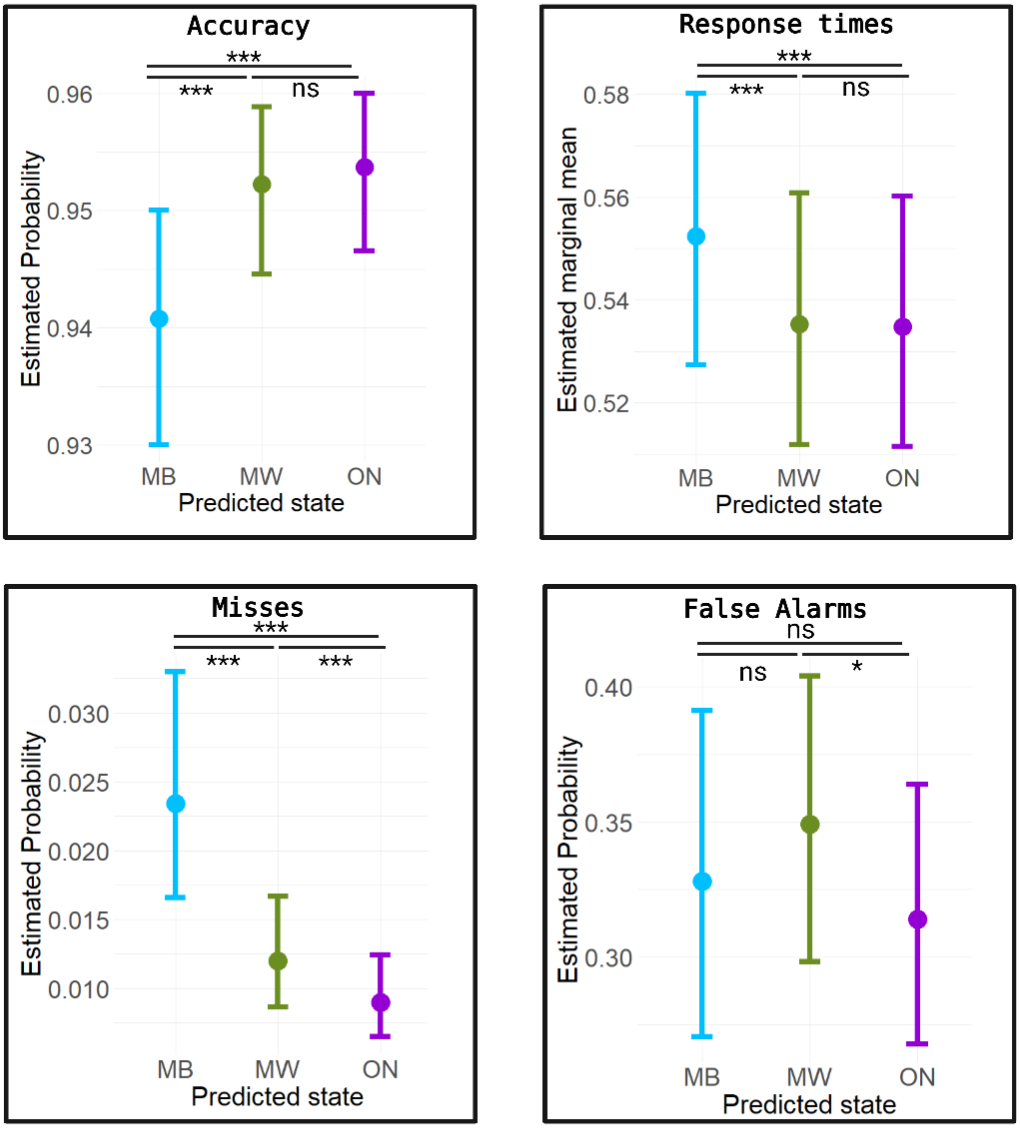

Figure 5: Trial-by-trial prediction of mind-state using a multivariate combination of neural markers. (A): Distribution of performances (balanced accuracy) of subject-level classifiers, both for true data and permuted data (mean score of 500 labels permutations). The classifier was trained and tested by cross-validation using labeled trials (<5 seconds before probe onsets). Spectral, complexity, connectivity, and ERP markers were used as raw features, followed by a dimensionality reduction by (non-linear) PCA. Left: performances for all subjects; right: performances for subjects presenting with the 3 mind states. Colored dots represent individual scores (one color per participant) (B): Behavioral markers as a function of the predicted mind state in non-labeled trials (>5s before probe onsets). (Binomial) linear mixed models were computed with predicted mind-state as the main explanatory factor, and subject ID as a random intercept. Statistical bars represent pairwise statistical comparisons between states. We found very similar behavioral patterns for predicted trials as compared to reported (labeled) trials.

The detailed statistical results can be found in Table S6.
***: FDR corrected p-value<0.001
*: FDR corrected p-value<0.05
n.s.: FDR corrected p-value>0.05

A. Exemples of transitions between mind states

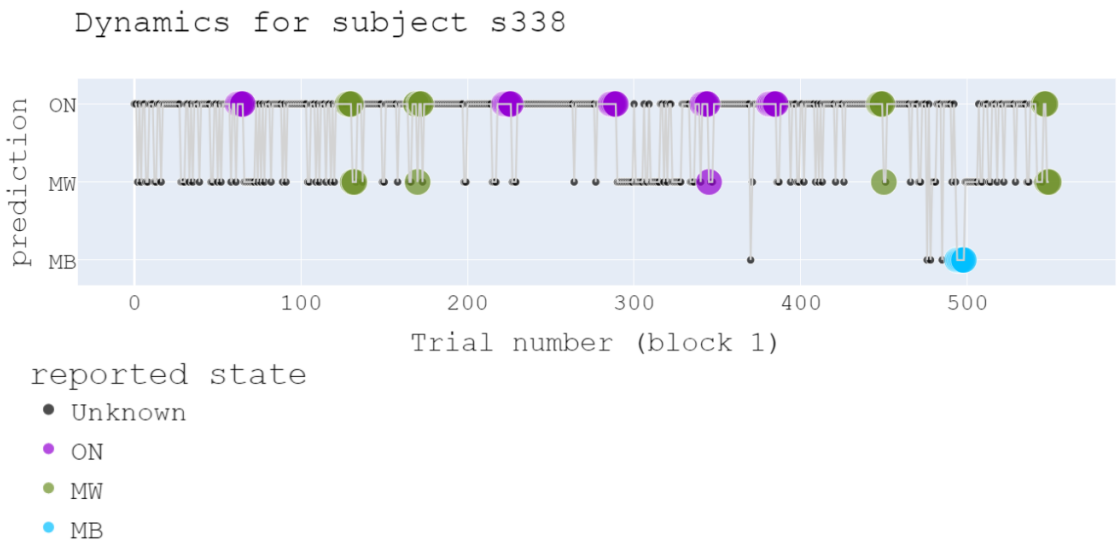

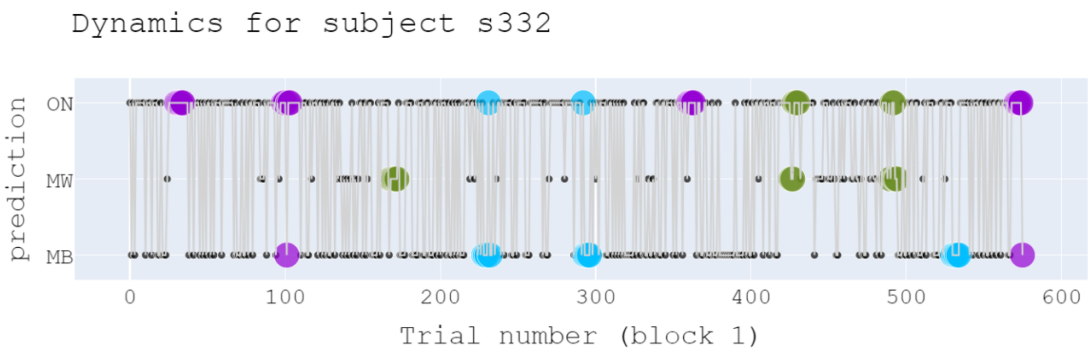

B. Transition probabilities among subjects having reported all mind-states

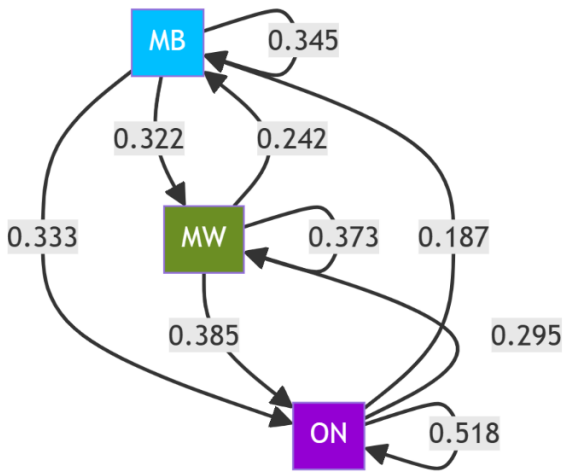

Figure 6: Transition dynamics between mind-states. (A): 2 examples of transitions between mind-states during one-block of the SART. The horizontal axis represents the trial number and the vertical axis the predicted mind state (by the classifier). Each dot represents a trial, with small black colors representing non-labeled trials and big colored dots representing labeled trials (blue: MB; purple: ON; green: MW). (B): Average transition probabilities for the 3 mind-states, computed across subjects presenting with the 3 mind-states. While MB frequency could be inflated due to methodological reasons, our results suggest that MB is a more frequent state than previously thought.

Source space wSMI

wSMI δ

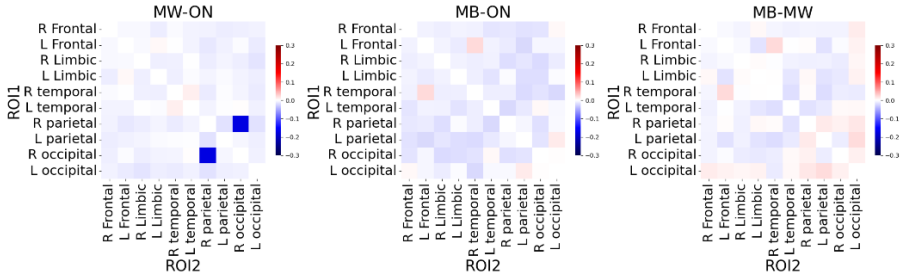

wSMI θ

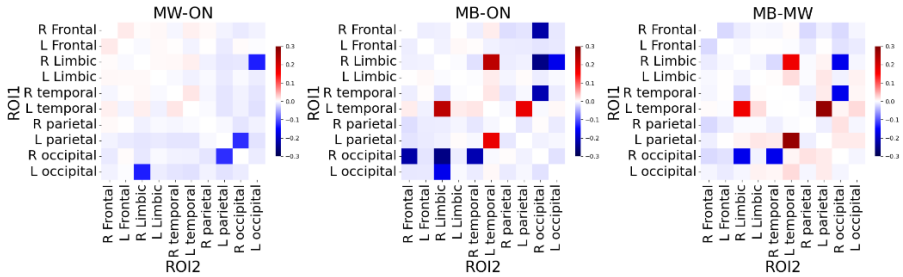

wSMI α

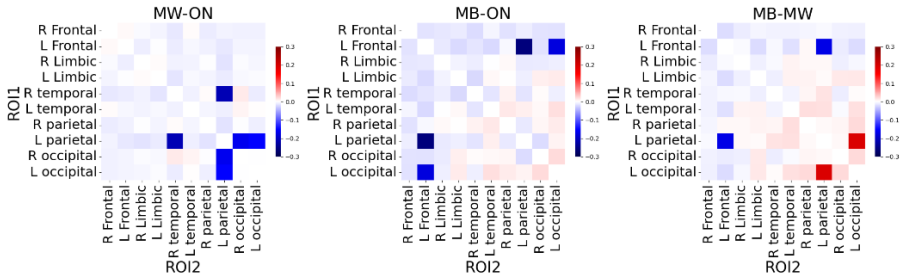

wSMI γ

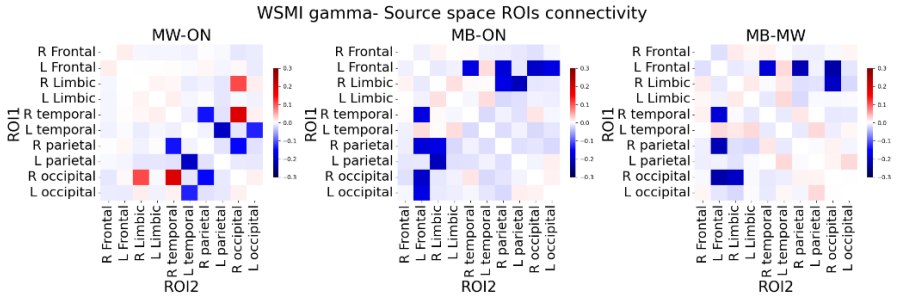

Fig S1: Source space wSMI computed at the delta, theta, alpha and gamma frequencies. Each square-matrix represents the contrast in connectivity, computed in source space, between two mind-states, for each pair of regions of interest (ROIs). Only significantly different connections (FDR corrected p-value<0.05) are highlighted, the other ones are masked. ANOVA tables for the statistical models can be found in Table 3. Specific decreases of connectivity between frontal and posterior regions were observed in the alpha, beta (Figure 3) and gamma bands.

δ: delta band; θ: theta band; α: alpha band; γ: gamma band
wSMI: weighted symbolic mutual information
R: right; L: left

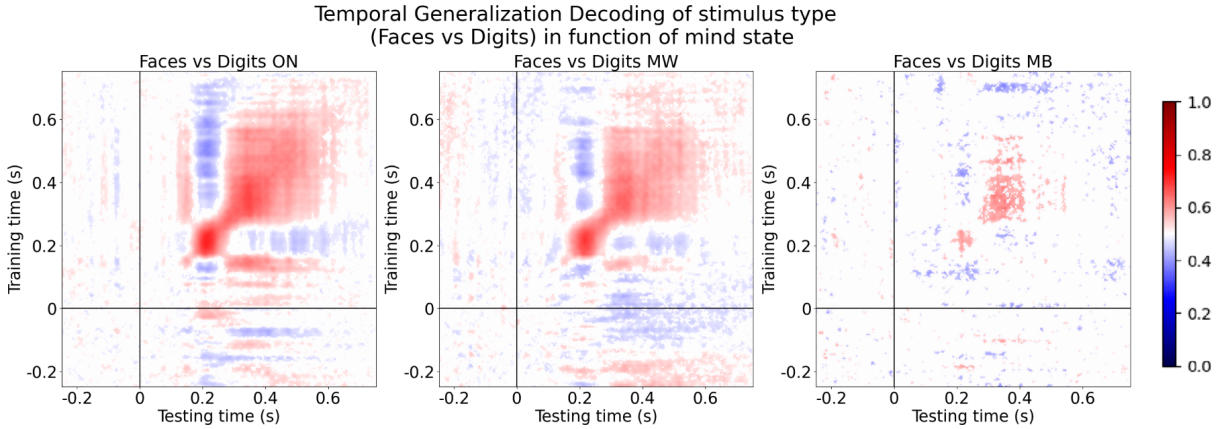

Fig S2: Temporal generalization decoding. Generalization matrix of decoding of a linear classifier trained to distinguish across time between face trials and digit trials. The classifier was trained at each time point independently using a 10-fold cross-validation, and then tested at every time point, obtaining thus a whole matrix of training times - testing times. The Classifier's performance was measured using the AUC (area under the ROC curve) at each point of the matrix, and then tested against chance level using a two-sided non-parametric sign test across validation folds, FDR-corrected for multiple comparisons (for n_times x n_times= 63 001 comparisons, alpha level = 0.05). Non-significant decoding points (FDR-corrected p-value>0.05) were masked. For both ON and MW conditions, we observed a very classical pattern of decoding, with an early diagonal pattern corresponding to a series of successive, transient and unconscious neural events, and a late and square-shape pattern corresponding to a sustained neural representation, this last pattern having been previously associated with conscious access. Crucially, for MB, decoding between stimuli-types was severely disturbed, with an incomplete but still visible early diagonal, and with a quasi-disappearance of the late pattern of decoding, suggesting a lack of conscious access to visual stimuli during MB trials.

Mental state	Accuracy (%)	FA (%)	Misses (%)	RTs (ms)
ON	96.5 ± 0.3	22.6 ± 2.1	0.8 ± 0.1	548 ± 13
MW	93.6 ± 0.5	42.2 ± 2.9	1.5 ± 0.3	536 ± 13
MB	92.7 ± 0.7	41.1 ± 3.7	2 ± 0.4	558 ± 14

Behavioral measure	Main effect of mind state		Pairwise contrasts
	χ^2	***FDR corrected p-value***	
Accuracy	χ^2 (2)=126.5	$3.52 * 10^{-15}$	MW *vs* ON : z-ratio=-10.064, p-value=0.00023 MB *vs* ON z-ratio=-9.133, p-value=0.00023 MB vs MW z-ratio=-1.6, p-value=0.13
FA	χ^2 (2)=77.7	$3.52 * 10^{-15}$	MW *vs* ON : z-ratio=9.7, p-value= 0.00023 MB *vs* ON: z-ratio=6.4, p-value= 0.00023 MB vs MW: z-ratio=-0.34, p-value=0.82
Misses	χ^2 (2)=50.4	$1.2 * 10^{-10}$	MW *vs* ON : z-ratio=5.38, p-value= 0.00023 MB *vs* ON: z-ratio=6.78, p-value= 0.00023 MB vs MW: z-ratio=2.39 p-value=0.027
RT	χ^2 (2)=35.5	$1.6 * 10^{-7}$	MW *vs* ON : z-ratio=4.34, p-value= 0.00023 MB *vs* ON: z-ratio=-2.40, p-value= 0.027 MB vs MW: z-ratio=-5.34 p-value=0.00023

Table 1: Behavioral results in labeled trials. Results of the linear mixed models with mind-state as a main factor and subject ID as a random intercept, for accuracy, false alarms (FA), misses and response times (RT). The table presents the model estimates for each mind-state (top) and the statistical contrasts (bottom). P-values were corrected for multiple comparisons using an FDR procedure.

Neural marker	Main effect of mind-state		Main effect of electrode location		Interaction mind-state*electrode	
	F(2)	FDR corrected p-value	F(63)	FDR corrected p-value	F(126)	FDR corrected p-value
Approximative Entropy	15,33	2.85e-07	382,95	0.00e+00	4,91	1.45e-65
Sample Entropy	16,08	1.38e-07	387,9	0.00e+00	4,98	5.10e-67
Kolmogorov	0,93	3.93e-01	385,03	0.00e+00	5,65	8.32e-82
Permutation Entropy alpha	8,65	2.02e-04	578,51	0.00e+00	11,25	4.64e-215
Permutation Entropy beta	9,04	1.38e-04	1050,62	0.00e+00	10,36	3.93e-193
Permutation Entropy delta	1,44	2.40e-01	92,66	0.00e+00	2,1	9.92e-12
Permutation Entropy gamma	14,64	5.65e-07	878,23	0.00e+00	8,37	3.47e-145
Permutation Entropy theta	7,96	3.95e-04	219,22	0.00e+00	2,18	6.21e-13
normalized PSD alpha	21,65	5.62e-10	675,29	0.00e+00	8,76	1.88e-154
normalized PSD beta	13,96	1.07e-06	266,19	0.00e+00	9,28	6.41e-167
normalized PSD delta	6,91	1.10e-03	100,62	0.00e+00	4,8	3.50e-63
normalized PSD gamma	1,77	1.76e-01	678	0.00e+00	7,64	8.33e-128
normalized PSD theta	3,24	4.12e-02	364,61	0.00e+00	5,74	6.42e-84
WSMI alpha	36,48	2.27e-16	9,83	9.45e-92	3,52	1.28e-36
WSMI beta	5,1	6.57e-03	25,06	0.00e+00	11,38	3.09e-218
WSMI delta	11,38	1.38e-05	11,79	5.76e-116	1,46	6.43e-04
WSMI gamma	14,53	6.17e-07	28,73	0.00e+00	11,25	4.57e-215
WSMI theta	77,39	4.19e-34	9,24	1.65e-84	1,26	2.72e-02
PLV	26,4	3.4e-12	648	0.00e+00	6,2	5.9e-94

Table 2: Neural markers results (sensor space). ANOVA tables of the statistical models computed for each neural marker in sensor space (linear mixed models with mind state, electrode location and their interaction as main factors, and subject ID as a random intercept). P-values were corrected for multiple comparisons using an FDR procedure.

Connectivity measure (source level)	Mind-state		connection		interaction	
	F(2)	FDR corrected p-value	F(44)	FDR corrected p-value	F(88)	FDR corrected p-value
wSMI alpha	17,95	3.00e-08	236,66	0.00e+00	1,27	4.60e-02
wSMI beta	36,76	2.75e-16	243,13	0.00e+00	1,75	2.29e-05
wSMI delta	21,71	8.04e-10	105,37	0.00e+00	0,66	9.94e-01
wSMI gamma	17,64	3.67e-08	247,8	0.00e+00	1,99	1.53e-07
wSMI theta	11,89	9.34e-06	137,94	0.00e+00	1,35	1.89e-02
PLV	8,1	2.9e-04	1181	0.00e+00	4,6	1.2e-41

Table 3: Source-level connectivity. ANOVA tables of the statistical models computed for each connectivity measure in source space (linear mixed models with mind state, connection ID and their interaction as main factors, and subject ID as a random intercept). P-values were corrected for multiple comparisons using an FDR procedure.

Time-window (s - s)	Mind-state		Channel		Interaction	
	F(2)	FDR corrected p-value	F(63)	FDR corrected p-value	F(126)	FDR corrected p-value
-0.025 - 0.025	0	1.00e+00	27,58	0.00e+00	0,38	1.00e+00
0.050 - 0.100	0	1.00e+00	34,56	0.00e+00	1,04	6.41e-01
0.125 - 0.175	0	1.00e+00	46,13	0.00e+00	1,39	5.04e-03
0.200 - 0.250	0	1.00e+00	12,33	5.63e-123	0,82	1.00e+00
0.275 - 0.325	0	1.00e+00	10,62	1.37e-101	0,62	1.00e+00
0.350 - 0.400	0	1.00e+00	16,01	1.27e-169	2,04	1.23e-10
0.425 - 0.475	0	1.00e+00	40,41	0.00e+00	4,48	2.54e-56
0.500 - 0.550	0	1.00e+00	56,67	0.00e+00	3,23	6.39e-31
0.575 - 0.625	0	1.00e+00	42,34	0.00e+00	3,25	3.17e-31
0.650 - 0.700	0	1.00e+00	23,94	0.00e+00	2,41	2.19e-16

Table 4 : Event related potentials (ERPs). ANOVA tables of the statistical models computed at each time window (linear mixed models with mind state, electrode location and their interaction as main factors, and subject ID as a random intercept). P-values were corrected for multiple comparisons using an FDR procedure.

Subject ID	True score	Mean permutation score	p-value
s304	0,48	0,33	<0,002
s305	0,41	0,33	0,02
s306	0,49	0,4	<0,002
s308	0,48	0,39	<0,002
s309	0,43	0,36	0,01
s310	0,45	0,33	<0,002
s311	0,42	0,34	0,01
s313	0,39	0,33	0,03
s315	0,54	0,45	<0,002
s317	0,44	0,4	0,03
s319	0,36	0,33	0,22
s320	0,38	0,34	0,09
s322	0,51	0,46	0,07
s323	0,45	0,34	<0,002
s324	0,5	0,43	0,02
s325	0,5	0,42	0,03
s328	0,58	0,46	<0,002
s329	0,48	0,43	0,01
s332	0,39	0,33	0,02
s338	0,59	0,56	0,15

Table 5: Permutation test results at subject level, for subjects with the 3 mind states

Predicted Mental state	Accuracy (%)	FA (%)	Misses (%)	RTs (ms)
ON	95.5 ± 0.3	32 ± 2.6	0.9 ± 0.1	545 ± 11
MW	95.1 ± 0.4	33 ± 2.7	1.2 ± 0.2	542 ± 11
MB	94.6 ± 0.5	33 ± 3	1.6 ± 0.3	548 ± 11

Behavioral measure	Main effect of mind state		Pairwise contrasts
	χ²	***FDR corrected p-value***	
Accuracy	χ^2 (2)=18.7	$1.54 * 10^{-4}$	MW *vs* ON : z-ratio=-0.8, p-value=0.47 MB *vs* ON z-ratio=--4.3, p-value=0.00015 MB vs MW z-ratio=--3.5, p-value=0.00074
FA	χ^2 (2)=6.7	0.036	MW *vs* ON : z-ratio=2.6, p-value= 0.012 MB *vs* ON: z-ratio=0.68, p-value= 0.52 MB vs MW: z-ratio=-0.93, p-value=0.39
Misses	χ^2 (2)=99	$2.5 * 10^{-15}$	MW *vs* ON : z-ratio=3.4, p-value= 0.00085 MB *vs* ON: z-ratio=9.9, p-value= 0.00015 MB vs MW: z-ratio=6.3, p-value=0.00015
RT	χ^2 (2)=44	$2.5 * 10^{-15}$	MW *vs* ON : z-ratio=-0.3, p-value= 0.78 MB *vs* ON: z-ratio=-6.5, p-value= 0.00015 MB vs MW: z-ratio=-5.9 p-value=0.00015

Table 6: Behavioral results in non-labeled trials in function of the predicted mind-state. Results of the linear mixed models with predicted mind-state as a main factor and subject ID as a random intercept, for accuracy, false alarms (FA), misses and response times (RT). The table presents the model estimates for each mind -state (top) and the statistical contrasts (bottom). P-values were corrected for multiple comparisons using an FDR procedure.